AN ABSTRACT FOR THE THESIS OF

Michael S. Boger for the degree of Master of Science in Electrical and Computer Engineering presented on July 6, 1994.

Title: General Pole Number Model of the Brushless Doubly-Fed Machine.

Abstract Approved: _____.
Dr. Alan K. Wallace

The Brushless Doubly-Fed Machine (BDFM) has the potential to be a more cost effective replacement for conventional induction or synchronous machine drives. The BDFM has two stator windings: a power winding and a control winding. An electronic power converter of variable voltage and frequency is connected to the control winding and allows the speed of the machine to be adjusted synchronously. The power winding, by design, carries the majority of the current needed for operation, the control winding only a fraction of the current, thus enabling the converter rating to be as low as 25% of the rating of the machine depending on the speed range of operation.

To date, only one specific stator pole-pair combination has been investigated, namely the 3/1 combination, where 3 and 1 refer to the power winding pole-pairs and the control winding pole-pair, respectively. Since the speed of the machine is dependent on the sum of the pole-pairs of the stator windings, a general pole numbered model is needed to evaluate the performance of such general machines with other pole-pair number machines. The BDFM describing system equations are transformed to the two axis (dq) rotor reference frame using a power invariant transformation. The analysis shows an additional term involving the common bar impedance which was not present in earlier analyses.

The dynamic model is simplified to yield a steady state synchronous model. The synchronous frequency of analysis is investigated which results in two equivalent steady state models. The models developed can easily handle excitation of any frequency or sequence on the control winding without the use of an auxiliary model as used in previous analyses. The voltage forced model predictions match data taken for a 5 hp BDFM laboratory prototype, establishing the validity of the analysis. The model is used in illustrating the torque producing capabilities and unity power factor operation of the machine under a variety of inputs. Using the model, predictions are made on a different pole-pair combination machine (4/2 BDFM) for use as a 60 hp pump drive as an alternative to a 3/1 BDFM for the same application.

General Pole Number Model of the Brushless Doubly-Fed Machine

by

Michael S. Boger

A THESIS

submitted to

Oregon State University

in partial fulfillment of
the requirements for the
degree of

Master of Science

Completed July 6, 1994

Commencement June 1995

APPROVED:

Redacted for Privacy

Professor of Electrical and Computer Engineering in charge of major

Redacted for Privacy

Head of Department of Electrical and Computer Engineering

Redacted for Privacy

Dean of Graduate School

Date thesis is presented: July 6, 1994.

Typed by Michael S. Boger for Michael S. Boger.

ACKNOWLEDGMENTS

Throughout my studies, I have received encouragement from many people. I first wish to thank my family for their moral support and words of praise. I dedicate this thesis to them. Thanks go to my major professor, Alan Wallace, who has helped guide my efforts and allowed me to concentrate on my work and develop new ideas. Thanks to professor G. Corwin Alexander for helping me hone my ability to present new ideas to others. Thanks to professor René Spee for his thoughts on machine design and special projects he has provided. Special thanks to all my fellow students who have always been there for the much needed attitude adjustments. We all learned new ideas from each other.

TABLE OF CONTENTS

LIST OF FIGURES

LIST OF TABLES

LIST OF SYMBOLS

B	damping coefficient
$\mathbf{C}$	general transformation matrix
$\mathbf{C}_r$	rotor transformation matrix (combined)
$\mathbf{C}_{rc}$	rotor transformation matrix used for rotor currents due to the control winding
$\mathbf{C}_{rp}$	rotor transformation matrix used for rotor currents due to the power winding
$\mathbf{C}_{sc}$	stator control winding transformation matrix
$\mathbf{C}_{sp}$	stator power winding transformation matrix
D_t	differentiation with respect to time
$\mathbf{f}_{abc}$	arbitrary abc domain variable
f_c	control winding supply frequency
f_p	power winding supply frequency
$\mathbf{f}_{qdo}$	arbitrary dq-axis variable
f_r	rotor frequency of rotation
$\mathbf{g}$	sub-matrix of $\mathbf{G}$
$\mathbf{G}$	impedance matrix that only includes resistive and constant inductive elements
$\mathbf{h}$	sub-matrix of $\mathbf{H}$
$\mathbf{H}$	impedance matrix that only includes rotor position dependent inductances
$\mathbf{i}_c$	control winding currents, abc or dq domain as specified
i_{dr}	d-axis rotor current (combined)
i_{drc}	d-axis rotor current due to the power winding
i_{drp}	d-axis rotor current due to the power winding
i_{0c}	0 sequence control winding current

i_{0p} 0 sequence power winding current

$\mathbf{i}_p$ power winding currents, abc or dq domain as specified

i_{qr} q-axis rotor current (combined)

i_{qrc} q-axis rotor current due to the control winding

i_{qrp} q-axis rotor current due to the power winding

$\mathbf{i}_r$ rotor currents, abc or dq domain as specified

$i_{r(i,j)}$ rotor current in loop i, nest j

$\mathbf{i}_{rc}$ rotor currents due to the control winding

$\mathbf{i}_{rp}$ rotor currents due to the power winding

$\mathbf{I}_c$ steady state control winding dq currents

$\tilde{I}_c$ rms value of the control winding dq currents

I_{dc} steady state d-axis control winding current

I_{dp} steady state d-axis power winding current

I_{dr} steady state d-axis rotor current

$\mathbf{I}_p$ steady state power winding dq currents

$\tilde{I}_p$ rms value of the power winding dq currents

I_{qc} steady state q-axis control winding current

I_{qp} steady state q-axis power winding current

I_{qr} steady state q-axis rotor current

$\mathbf{I}_r$ steady state rotor dq currents

$\tilde{I}_r$ rms value of the rotor dq currents

Im imaginary part of a complex variable

j complex number operator

J moment of inertia

L_{ii} rotor self-impedance of a loop

L'_{11} leakage reactance of the common nest bar

L_{mc} control winding magnetizing self-inductance per phase

L_{lc} control winding leakage inductance per phase

L_{mp} power winding magnetizing self-inductance per phase

L_{lp} power winding leakage inductance per phase

L_c control winding dq equivalent inductance

L_p power winding dq equivalent inductance

L_r dq equivalent rotor inductance

$\mathbf{L}_{scr}$ mutual inductance matrix between the control winding and the rotor

$\mathbf{L}_{scri}$ mutual inductance matrix between the i-th rotor loop and the control winding

L_{scri} peak mutual inductance between the i-th rotor loop and the control winding

$\mathbf{L}_{spr}$ mutual inductance matrix between the power winding and the rotor

L_{spri} peak mutual inductance between the i-th rotor loop and the power winding

$\mathbf{L}_{spri}$ mutual inductance matrix between the i-th rotor loop and the power winding

L'_{11} common bar inductance of a nest

m number of rotor loops

M_{ij} mutual inductance between the i and j loops of the rotor in the same nest

M'_{ij} mutual impedance between the i and j loops of the rotor in a different nest

M_c dq equivalent mutual inductance between the control winding and the rotor

M_p dq equivalent mutual inductance between the power winding and the rotor

n number of rotor nests = $P_p + P_c$

P_p power winding pole pairs

P_c control winding pole pairs

Q_p slots/pole/phase of the power winding

Q_c slots/pole/phase of the control winding

r_c control winding phase resistance

r_p power winding phase resistance

r_{ii} rotor loop resistance

r_{11} resistance of the common nest bar

r_{ij} rotor common resistance of the shared end ring

r_r dq equivalent rotor resistance

Re real part of a complex variable

S number of stator slots

T_e electrical torque

T_l load torque

$\mathbf{U}_3$ identity matrix of order 3

v_{0c} 0 sequence control winding voltage

v_{0p} 0 sequence power winding voltage

v_c instantaneous control winding dq voltages

$\mathbf{v}_c$ control winding dq domain voltages

v_{dc} d-axis control winding voltage

v_{dp} d-axis power winding voltage

v_p instantaneous power winding dq voltages

$\mathbf{v}_p$ power winding dq domain voltages

v_{qc} q-axis control winding voltage

v_{qp} q-axis power winding voltage

$\mathbf{v}_{sc}$ control winding voltages in the abc domain

$\mathbf{v}_{sp}$ power winding voltages in the abc domain

$\mathbf{v}_{r}$ rotor voltages, dq or abc domain as specified

V_{Ac} a-phase control winding voltage

V_{Ap} a-phase power winding voltage

V_{Bc} b-phase control winding voltage

V_{Bp} b-phase power winding voltage

$\mathbf{V}_{c}$ steady state dq control winding voltages

V_{Cc} c-phase control winding voltage

V_{Cp} c-phase power winding voltage

$\hat{V}_{c}$ peak value of the control winding abc domain voltages

V_{dc} steady state d-axis control winding voltage

V_{dp} steady state d-axis power winding voltage

$\hat{V}_{p}$ peak value of the power winding abc domain voltages

$\mathbf{V}_{p}$ steady state dq power winding voltages

V_{qc} steady state q-axis control winding voltage

V_{qp} steady state q-axis power winding voltage

$\mathbf{Z}_{ij}$ rotor loop impedance sub-matrix

$\mathbf{Z}_{r}$ total rotor impedance matrix

$\mathbf{Z}_{sc}$ control winding impedance matrix

$\mathbf{Z}_{scr}$ mutual impedance matrix between the control winding and the rotor

$\mathbf{Z}_{sp}$ power winding impedance matrix

$\mathbf{Z}_{spr}$ mutual impedance matrix between the power winding and the rotor

α mechanical displacement between a-phases of the power and control windings

ϕ_c phase angle of the control winding dq currents with respect to the power winding a-phase voltage

ϕ_{cp} time zero offset angle between the power and control winding voltages

ϕ_p phase angle of the power winding dq currents with respect to the power winding a-phase voltage

ϕ_r phase angle of the rotor dq currents with respect to the power winding a-phase voltage

$\Gamma^{\pm}$ electrical power angle for positive or negative sequence

θ_r rotor mechanical angle

Ψ arbitrary phase angle

ω_c angular frequency of the control winding voltages

ω_p angular frequency of the power winding voltages

ω_r angular frequency of the rotor shaft

ω_R angular frequency of the currents in the rotor during synchronous operation

GENERAL POLE NUMBER MODEL OF THE BRUSHLESS DOUBLY-FED MACHINE

1. INTRODUCTION

Recently, there have been noticeable interest and research activities in using brushless doubly-fed reluctance machines [1,2] and brushless doubly-fed induction machines [3,4] for adjustable speed drives (ASD) and variable speed generation (VSG). The brushless doubly-fed induction machine (BDFM) shows great promise in reducing the rating of the power electronic converter needed for ASD and VSG applications to a small fraction of the machine rating. Early work dealt with two separate wound rotor induction machines cascaded together [5] to provide speed control. The BDFM [6,7] eliminates the need for a wound rotor induction machine, and when used with a bi-directional power electronic converter, has the ability to provide precise speed control by virtue of its two stator windings and modified cage rotor. The BDFM shows promising results in automotive, wind generation, and pump drive applications, as well as other variable speed niche applications [3].

Stator pole-pair combinations investigated to date include 2/1, 3/1, and 6/2, with 2, 3 and 6 power winding pole-pairs and 1 and 2 control winding pole-pairs, respectively. However, to date, two axis model development has addressed the 3/1 geometry exclusively [8-10]. Investigations of other pole-pair combinations has been hampered by the lack of a general pole number model. Designs other than the 3/1 have been based on intuition and simplistic induction motor equations; focused optimization of these other designs has not been possible. The general pole number model facilitates the design and optimization of alternate pole combination machines. The expanded choice of pole combinations allows for flexible designs enabling tailoring of the drive to custom speed ranges and torque requirements.

The analysis of the 3/1 machine results in a very simplified model because there are only four rotor nests which, when analyzed in a two axis reference frame, results in immediate orthogonalities. This thesis extends the modeling technique to any number of poles, enabling accurate design of new proposed BDFMs. The model shows the inclusion of terms in the mutual inductance parameters which did not appear in the 3/1 model because of cancellation due to the orthogonal axes of the 3/1 machine's rotor. Without this model, there can only be rough calculations based on classical induction motor equations which do not adequately define the relationship between two stator windings sharing a common nested loop rotor. In addition, this model can be easily extended to handle cage-less BDFM rotors, where a cage-less rotor has only one common endring. This general pole model, in two axes, will result in a reduced simulation time due to a reduction of the number of state equations needing to be solved in comparison to a detailed simulation [11]. A power invariant d-q transformation is applied in the rotor reference frame to the voltage equations to arrive at the simplified model.

The dynamic model of the BDFM is simplified to a steady state synchronous model which enables steady state performance predictions. In addition, the capabilities of the machine can quickly be seen through a steady state analysis. The equivalent steady state model is in the rotor reference frame, however, the two axis voltages and currents are easily translated to terminal quantities through a scaling factor.

This thesis will describe the basic structure of the BDFM. Once the vernacular is explained, the describing impedance functions of the machine are derived. The BDFM system voltage equations are transformed to the two axis rotor reference frame through the application of three transformation matrices. This results in a dynamic model which can be converted to a steady state synchronous model. The model is validated by comparison with test data of a 5 hp laboratory prototype BDFM. Performance predictions of a proposed 60 hp pump drive are made for two alternate BDFM designs, a 3/1 and a

4/2 machine. Finally, the utility of the model in establishing the machine capabilities is demonstrated.

2. BDFM STRUCTURE

Externally, the BDFM looks like a standard induction machine, the only noticeable difference being the presence of an extra stator winding. It will use the same standard frame sizes any other electric motor would use. With the use of a power converter, the BDFM is designed to operate at a controllable synchronous speed as dictated by the following formula [8, 10, 11]:

$$f_r = \frac{f_p \pm f_c}{P_p + P_c} \tag{2-1}$$

where the sign on the control winding frequency denotes either positive sequence (+) or negative sequence (-) with respect to the power winding. This formula will be proven in a later chapter.

The BDFM has the potential to be economically viable in medium to high power drive applications due to the reduced cost of the converter needed to run the BDFM as a synchronous machine. In order to provide a base for further discussion, the machine structure and peculiar construction methods are described.

2.1. Stator Structure

The BDFM is wound with two separate three phase windings: the power and the control winding. These windings have different pole-pair numbers, P_p and P_c, respectively. A particular BDFM is referred to by its combination of power winding pole-pairs and control winding pole-pairs. For example, a 3/1 machine has 3 pole-pairs on the power winding and 1 pole-pair on the control winding. Normally, the number of power winding poles is greater than the control winding poles. No generality is lost by this assumption. A system diagram of the BDFM is shown in Fig. 2-1.

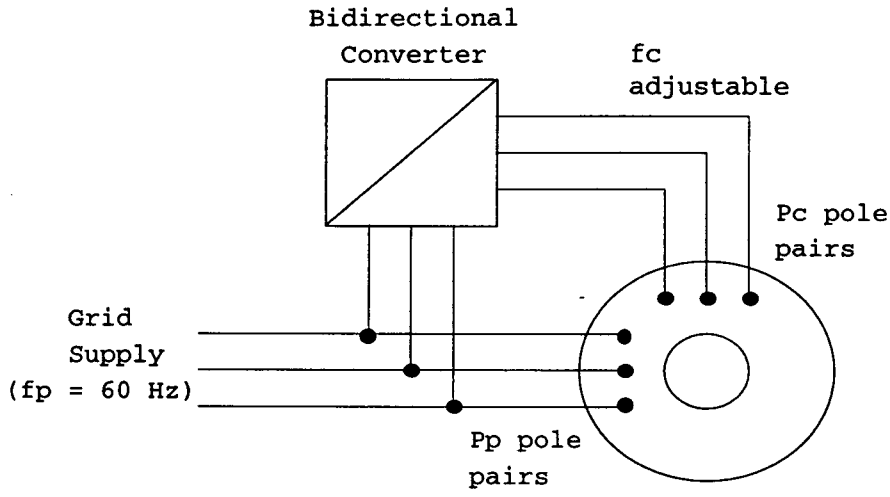

Figure 2-1. BDFM system diagram

The power winding is designed to have more poles than the control winding since the power winding is designed to handle the bulk of the power processed by the BDFM. In addition, the number of stator slots per pole is less for the power winding than for the control winding because of the greater number of poles on the power winding. The power winding is connected directly to the power grid, by definition. To date, BDFM ASDs that utilize either 230 V or 460 V have been designed and constructed.

The control winding is connected to a power converter of adjustable/controllable frequency and voltage. The control winding, by design, handles only a fraction of the current of the power winding of the machine. This results in a decreased rating, and hence, lower cost of power converter needed to operate the BDFM as an ASD or VSG compared to an induction or conventional synchronous machine system. For limited speed operation, the converter rating is unlikely to be greater than 50% of the power winding rating. Depending on the speed range, the converter rating may be as low as 25% of the rating of the power winding.

Controlling the excitation level of the control winding of the BDFM is similar to adjusting the field current applied to a conventional synchronous machine. Viewing the control winding as an equivalent field winding for the BDFM helps in understanding the operation of the machine. The differences are that the control winding of the BDFM is in the stator and has ac excitation; the field winding in a synchronous machine is on the rotor and is excited by dc. The level of excitation on the control winding can control the power factor of the power winding making it possible to run the BDFM in a unity, or even leading, power factor condition. These features make the BDFM very appealing with the tighter restrictions on harmonic pollution and the penalties imposed on industry for operating machinery with a poor power factor.

The stator windings are normally double layered windings of fractional pitch. Fractional pitch windings are used to reduce the amount of copper used in the manufacturing process and to approximate sinusoidal distribution with multiple identical coils. Given the winding diagram and the dimensions of the machine, the parameters of the machines, such as resistance and inductance, can be estimated from classical induction motor theory. For simplicity in analysis, only integral slot per pole per phase windings have been assumed. This eliminates potentially troublesome sub-harmonics introduced by fractional slot windings. Using integral slot windings and specifying the number of slots per pole per phase on the power winding, Q_p, fixes the number of slots per pole of the control winding, Q_c, and the number of stator slots, S. This distribution of the windings is important in the design and construction of the machine. Table 2-1 shows possible numbers of stator slots for three combinations of pole-pairs.

Table 2-1. Fixing of the control winding distribution and stator slots by choice of the pole pairs and power winding distribution

Pp	Pc	Qp	Qc	S
3	1	1	3	18
3	1	2	6	36
3	1	3	9	54
3	1	4	12	72
3	1	5	15	90
4	1	1	4	24
4	1	2	8	48
4	1	3	12	72
4	1	4	16	96
4	1	5	20	120
4	2	1	2	24
4	2	2	4	48
4	2	3	6	72
4	2	4	8	96
4	2	5	10	120

2.2. Rotor Structure

The rotor of the BDFM, unique to this machine, is based on work done by Creedy [12] and Broadway [7]. Similar to an induction machine, the rotor is normally non-salient. The rotor may be either caged or cage-less. A caged rotor has two common endrings with isolated loops that share only one of the endrings. A cage-less rotor has only one common endring; all loops are isolated on the other end. Both forms of the rotor have an endring that all of the loops share.

The rotor has m loops within n nests such than $n = P_p + P_c$. The loops of the rotor are numbered starting from the common loop, if present, and working inwards. All similar loops within a nest are numbered in the same way. Fig. 2-1 shows one nest of a BDFM caged rotor.

Depending on the pole-pairs of the windings, there will be different numbers of nests. For example, a 3/1 machine requires 4 nests; a 4/2 machine requires 6 nests. An illustration showing the isolated endrings of a cage-less rotor is shown in Fig. 2-3.

The rotor bars may either be placed in the slots, or the entire nest structure may be die cast. The laboratory prototype BDFM, for example, uses American Wire Gage (AWG) #4 bar for the loops. However, a 60 hp pump drive BDFM, soon to be installed in a municipal waste water treatment plant, will have a die cast rotor of an aluminum alloy. It is anticipated that this ability to manufacture the rotor through a die cast process will make the BDFM competitive with the induction machine for the adjustable speed drive market.

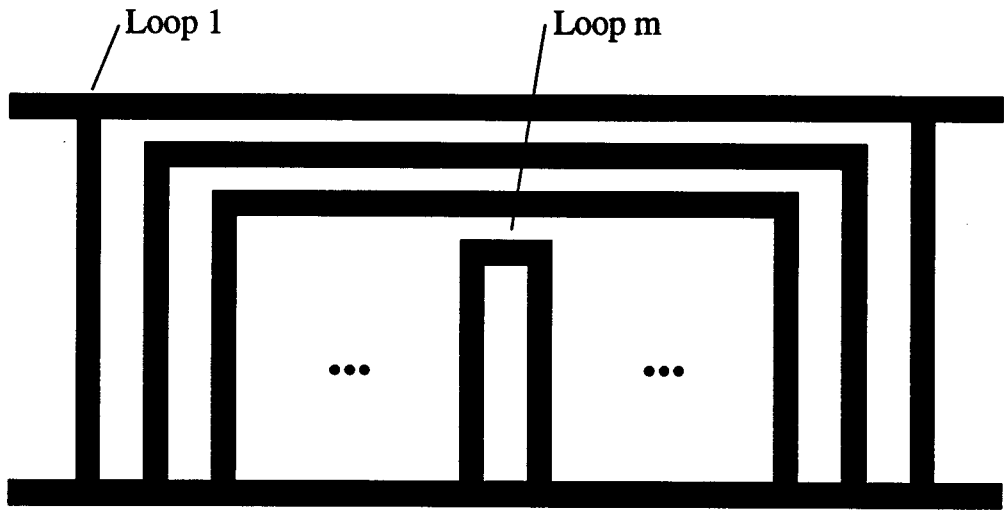

Figure 2-2. One nest of a BDFM Caged rotor showing loop numbering

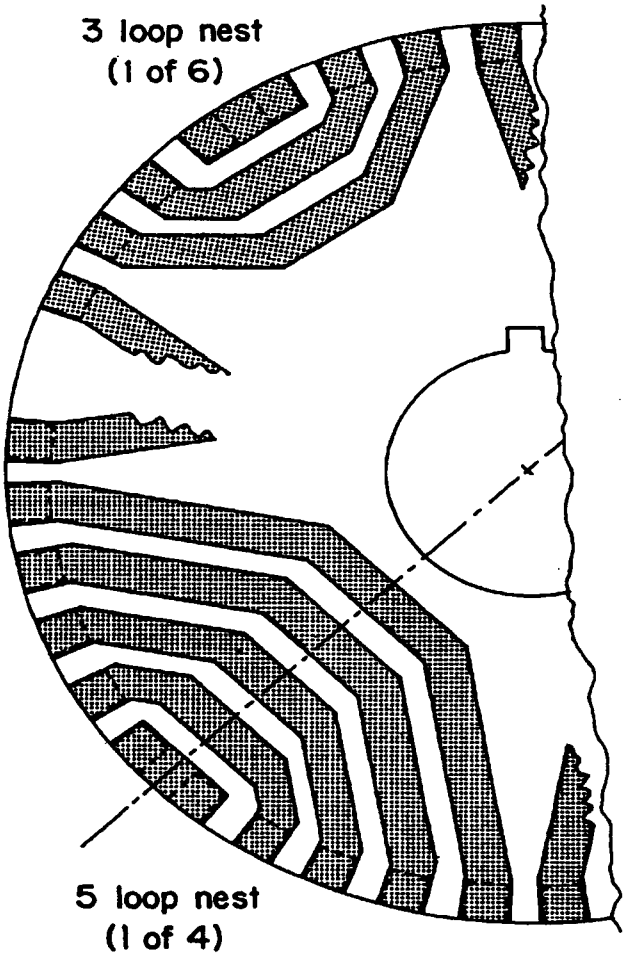

Figure 2-3. Isolated endrings of a 3/1 and a 4/2 BDFM

3. IMPEDANCE MATRICES

The impedances of each of the stator windings are determined based on the distribution of the three phase windings around the stator. The axes of each of the phases are assumed to be 120 electrical degrees apart. The rotor impedance functions are derived based on the geometry of the rotor, accounting for the nesting of the rotor loops. The rotor is assumed to be non-salient. The impedance functions are known as the 'abc' quantities since they refer to the actual phases of the machines and, in the case of the rotor, to the actual loops of the rotor. These abc quantities are subsequently transformed into the direct-quadrature (dq) reference frame which rotates at the mechanical velocity of the rotor. This reference frame is referred to as the rotor reference frame; the transformed quantities are called 'dq' quantities.

The abc voltage equation [8,10], (3-1), delineates the particular impedance functions that must be derived. Once the impedance functions are determined, they can be transformed to the dq rotor reference frame. There is assumed to be no direct coupling between the power and control windings due to the different pole numbers on each of the windings. Coupling is assumed to occur only through the rotor, as represented by the zero entries in (3-1).

$$\begin{bmatrix} \mathbf{v}_{sp} \\ \mathbf{v}_{sc} \\ \mathbf{v}_{r} \end{bmatrix} = \begin{bmatrix} \mathbf{Z}_{sp} & \mathbf{0} & \mathbf{Z}_{spr} \\ \mathbf{0} & \mathbf{Z}_{sc} & \mathbf{Z}_{scr} \\ \mathbf{Z}_{spr}^{t} & \mathbf{Z}_{scr}^{t} & \mathbf{Z}_{r} \end{bmatrix} \begin{bmatrix} \mathbf{i}_{sp} \\ \mathbf{i}_{sc} \\ \mathbf{i}_{r} \end{bmatrix} \tag{3-1}$$

3.1. Stator Impedances

The power winding impedance matrix, (3-2), is independent of the rotor position due to the non-salient rotor. This matrix resembles the stator impedance matrix of a

standard induction machine [17]. The self impedance terms are located along the diagonal and include the leakage inductance of the winding.

$$\mathbf{Z}_{sp} = \begin{bmatrix} r_p + D_t\left(L_{mp} + L_{lp}\right) & -\frac{1}{2}D_t L_{mp} & -\frac{1}{2}D_t L_{mp} \\ -\frac{1}{2}D_t L_{mp} & r_p + D_t\left(L_{mp} + L_{lp}\right) & -\frac{1}{2}D_t L_{mp} \\ -\frac{1}{2}D_t L_{mp} & -\frac{1}{2}D_t L_{mp} & r_p + D_t\left(L_{mp} + L_{lp}\right) \end{bmatrix} \tag{3-2}$$

The control winding impedance matrix, (3-3), resembles the power winding impedance matrix. The values of the inductances in both matrices can be determined by classical methods based on induction machine theory [13-17].

$$\mathbf{Z}_{sc} = \begin{bmatrix} r_c + D_t\left(L_{mc} + L_{lc}\right) & -\frac{1}{2}D_t L_{mc} & -\frac{1}{2}D_t L_{mc} \\ -\frac{1}{2}D_t L_{mc} & r_c + D_t\left(L_{mc} + L_{lc}\right) & -\frac{1}{2}D_t L_{mc} \\ -\frac{1}{2}D_t L_{mc} & -\frac{1}{2}D_t L_{mc} & r_c + D_t\left(L_{mc} + L_{lc}\right) \end{bmatrix} \tag{3-3}$$

3.2. Rotor Impedances

The rotor impedance matrices are rather elaborate since they must include the mutual inductances between any and every loop with all other loops on the rotor. In addition, the presence of a common endring necessitates the use of a common resistance which is used to compensate for the other currents that are also flowing in the endring when writing the electrical mesh current equations which describe the rotor. When using a caged rotor, the common nest bar impedance must also be included in the impedance; this consists of the bar resistance and the slot leakage inductance.

The total rotor impedance matrix is partitioned into sub-matrices. These sub-matrices group all of the impedances associated with a particular loop number. There are assumed to be *n* nests, each consisting of *m* loops. Therefore, each sub-matrix is square of order *n*, and the complete rotor impedance matrix, (3-4), is square of dimension *mn*.

$$\mathbf{Z}_r = \begin{bmatrix} \mathbf{Z}_{11} & \mathbf{Z}_{12} & \cdots & \mathbf{Z}_{1m} \\ \mathbf{Z}_{21} & \mathbf{Z}_{22} & \cdots & \mathbf{Z}_{2m} \\ \vdots & \vdots & \ddots & \vdots \\ \mathbf{Z}_{m1} & \mathbf{Z}_{m2} & \cdots & \mathbf{Z}_{mm} \end{bmatrix} \tag{3-4}$$

The indices in (3-4) refer to a specific loop. The off-diagonal terms group the mutual inductance terms from loops *j* to loops *i*. Loops are numbered in a nest starting from the outer loop, working inwards. If the rotor has a cage, the cage bar is loop *1*. The impedance matrix for the caged rotor terms [8,10], (3-5), includes the effects of the shared bar impedance.

$$\mathbf{Z}_{11} = \begin{bmatrix} r_{11} + D_t L_{11} & -r_{11}' - D_t\left(L_{11}' + M_{11}\right) & -D_t M_{11} & \cdots & -r_{11}' - D_t\left(L_{11}' + M_{11}\right) \\ -r_{11}' - D_t\left(L_{11}' + M_{11}\right) & r_{11} + D_t L_{11} & -r_{11}' - D_t\left(L_{11}' + M_{11}\right) & \cdots & -D_t M_{11} \\ -D_t M_{11} & -r_{11}' - D_t\left(L_{11}' + M_{11}\right) & r_{11} + D_t L_{11} & \cdots & -D_t M_{11} \\ \vdots & \vdots & \vdots & \ddots & \vdots \\ -r_{11}' - D_t\left(L_{11}' + M_{11}\right) & -D_t M_{11} & -D_t M_{11} & \cdots & r_{11} + D_t L_{11} \end{bmatrix} \tag{3-5}$$

If the rotor were cage-less, the impedance matrix would be like the other diagonal matrices in (3-4) as shown below.

$$\mathbf{Z}_{ii} = \begin{bmatrix} r_{ii} + D_t L_{ii} & -D_t M_{ii} & \cdots & -D_t M_{ii} \\ -D_t M_{ii} & r_{ii} + D_t L_{ii} & \cdots & -D_t M_{ii} \\ \vdots & \vdots & \ddots & \vdots \\ -D_t M_{ii} & -D_t M_{ii} & \cdots & r_{ii} + D_t L_{ii} \end{bmatrix} \tag{3-6}$$

Equation (3-7) shows an off diagonal impedance matrix of (3-4) which includes the common resistance of the shared endring and the mutual inductance between the same loop number in the same nest and from different nests. The common resistance term is used to describe the currents in the shared endring.

$$\mathbf{Z}_{ij} = \begin{bmatrix} r_{ij} + D_t M_{ij} & -D_t M_{ij}^{'} & \cdots & -D_t M_{ij}^{'} \\ -D_t M_{ij}^{'} & r_{ij} + D_t M_{ij} & \cdots & -D_t M_{ij}^{'} \\ \vdots & \vdots & \ddots & \vdots \\ -D_t M_{ij}^{'} & -D_t M_{ij}^{'} & \cdots & r_{ij} + D_t M_{ij} \end{bmatrix} \tag{3-7}$$

3.3. Stator-Rotor Mutual Impedances

The mutual impedance between one winding and the rotor is analyzed by considering the effects of a particular loop number in all nests. Each set of similar rotor loops is similarly analyzed. The complete mutual inductance matrices between the windings and the rotor are shown in (3-8) and (3-9).

$$\mathbf{Z}_{spr} = D_t \mathbf{L}_{spr} = D_t \begin{bmatrix} \mathbf{L}_{spr1} & \mathbf{L}_{spr2} & \cdots & \mathbf{L}_{sprm} \end{bmatrix} \tag{3-8}$$

$$\mathbf{Z}_{scr} = D_t \mathbf{L}_{scr} = D_t \begin{bmatrix} \mathbf{L}_{scr1} & \mathbf{L}_{scr2} & \cdots & \mathbf{L}_{scrm} \end{bmatrix} \tag{3-9}$$

In order to maintain a common reference for all measurements, the impedances are written in terms of mechanical angles. Each nest, and, hence, each specific rotor loop are spaced $2\pi/n$ mechanical radians from the nest proceeding. This spacing is translated into the equivalent electrical spacing of the winding by multiplying the rotor nest displacement by the winding's pole pairs. An examples of the power winding component mutual inductance matricx is shown in (3-10) where θ_r is the physical rotor position.

$$\mathbf{L}_{spri} = M_{spri}\begin{bmatrix} \cos(P_p\theta_r) & \cos\left(P_p\left(\theta_r+\frac{2\pi}{n}\right)\right) & \cdots & \cos\left(P_p\left(\theta_r+\frac{(n-1)2\pi}{n}\right)\right) \\ \cos\left(P_p\left(\theta_r-\frac{2\pi}{3P_p}\right)\right) & \cos\left(P_p\left(\theta_r-\frac{2\pi}{3P_p}+\frac{2\pi}{n}\right)\right) & \cdots & \cos\left(P_p\left(\theta_r-\frac{2\pi}{3P_p}+\frac{(n-1)2\pi}{n}\right)\right) \\ \cos\left(P_p\left(\theta_r-\frac{4\pi}{3P_p}\right)\right) & \cos\left(P_p\left(\theta_r-\frac{4\pi}{3P_p}+\frac{2\pi}{n}\right)\right) & \cdots & \cos\left(P_p\left(\theta_r-\frac{4\pi}{3P_p}+\frac{(n-1)2\pi}{n}\right)\right) \end{bmatrix} \tag{3-10}$$

The control winding mutual inductance matrix has an arbitrary offset angle, α, to account for any offset between the a-phases of the two stator winding systems. This angle is a physical angle extracted from the winding diagram as shown in Fig. 3-1. Once chosen, the angle will enable the alignment of the two winding's q-axes.

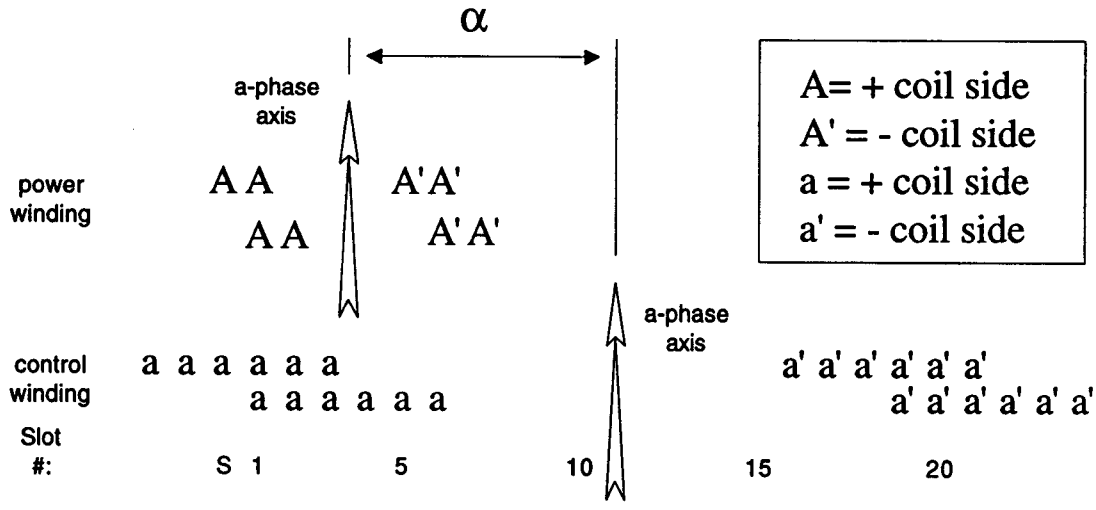

Figure 3-1. Portion of a winding diagram showing the relative displacement between the a-phases of the two windings

An examples of the control winding component mutual inductance matricx, incorporating the physical displacement angle, α, is shown in (3-11).

$$\mathbf{L}_{scri} = M_{scri}\begin{bmatrix} \cos(P_c(\theta_r-\alpha)) & \cos\left(P_c\left(\theta_r-\alpha+\frac{2\pi}{n}\right)\right) & \cdots & \cos\left(P_c\left(\theta_r-\alpha+\frac{(n-1)2\pi}{n}\right)\right) \\ \cos\left(P_c\left(\theta_r-\alpha-\frac{2\pi}{3P_c}\right)\right) & \cos\left(P_c\left(\theta_r-\alpha-\frac{2\pi}{3P_c}+\frac{2\pi}{n}\right)\right) & \cdots & \cos\left(P_c\left(\theta_r-\alpha-\frac{2\pi}{3P_c}+\frac{(n-1)2\pi}{n}\right)\right) \\ \cos\left(P_c\left(\theta_r-\alpha-\frac{4\pi}{3P_p}\right)\right) & \cos\left(P_c\left(\theta_r-\alpha-\frac{4\pi}{3P_c}+\frac{2\pi}{n}\right)\right) & \cdots & \cos\left(P_c\left(\theta_r-\alpha-\frac{4\pi}{3P_c}+\frac{(n-1)2\pi}{n}\right)\right) \end{bmatrix} \tag{3-11}$$

Once all of the impedance matrices have been determined, the machine performance can be determined through simulation.. However, the resultant electrical system needed to describe the BDFM is of order 6+*mn*. For even a moderate sized BDFM, this results in a substantial coding and simulation effort. In order to speed the simulation process, the system equations are transformed to the dq domain which will reduce the order of the electrical system to 6.

4. TRANSFORMATION MATRICES

The dq mechanical rotor reference frame is a convenient frame to analyze the BDFM because it simplifies the impedance functions. A modified, power invariant, Park's transformation is applied which will ensure simplified torque and power equations. A general transformation matrix that encompasses multiple harmonics given in [18] can be simplified to analyze only the fundamental effects of the stator windings and the rotor nests. Because the matrix is both orthogonal and power invariant [26],

$$\mathbf{C}^{-1} = \mathbf{C}^{T}. \tag{4-1}$$

The transformation matrix, **C**, is defined such that an arbitrary abc variable can be transformed to the dq reference frame as shown in (4-2). A graphical representation of the transformation is shown in Fig. 4-1.

$$\mathbf{f}_{qdo} = \mathbf{C}\mathbf{f}_{abc} \tag{4-2}$$

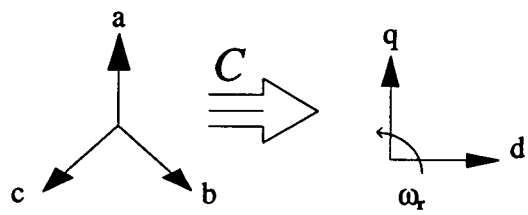

Figure 4-1. Graphical depiction of three phase to dq rotor reference frame transformation

The transformation process is taken in steps. Each winding is translated to the rotor reference frame separately. The rotor is then translated to the reference frame through the use of two separate matrices so that the effect from both windings can be included. This process will, in effect, establish two dq reference frames, superimposed on each other, which rotate at the speed of the rotor. There is assumed to be no direct coupling between the two stator windings; coupling from one winding to the other occurs only through the rotor. The applied voltages are assumed to be sinusoidal so that only the fundamental of each need be analyzed.

4.1. Stator Transformation

Transformation of the two stator windings is accomplished through the application of separate transformation matrices. The power winding stator transformation, (4-3), resolves the three phases of the power winding onto two orthogonal axes. These axes are locked onto the rotor by inclusion of the rotor angle, θ_r.

$$\mathbf{C}_{sp} = \sqrt{\frac{2}{3}}\begin{bmatrix} \cos(P_p\theta_r) & \cos\left(P_p\left(\theta_r - \frac{2\pi}{3P_p}\right)\right) & \cos\left(P_p\left(\theta_r - \frac{4\pi}{3P_p}\right)\right) \\ \sin(P_p\theta_r) & \sin\left(P_p\left(\theta_r - \frac{2\pi}{3P_p}\right)\right) & \sin\left(P_p\left(\theta_r - \frac{4\pi}{3P_p}\right)\right) \\ \sqrt{\frac{1}{2}} & \sqrt{\frac{1}{2}} & \sqrt{\frac{1}{2}} \end{bmatrix} \tag{4-3}$$

In order to align the q-axes of both systems, a mechanical offset angle, α, is introduced which is defined as the angle between the a-phases of the two windings as defined in the previous chapter. The control winding transformation, (4-4), shows the inclusion of this angle.

$$\mathbf{C}_{sc} = \sqrt{\frac{2}{3}} \begin{bmatrix} \cos\left(P_c(\theta_r - \alpha)\right) & \cos\left(P_c\left(\theta_r - \alpha - \frac{2\pi}{3P_p}\right)\right) & \cos\left(P_c\left(\theta_r - \alpha - \frac{4\pi}{3P_p}\right)\right) \\ \sin\left(P_c(\theta_r - \alpha)\right) & \sin\left(P_c\left(\theta_r - \alpha - \frac{2\pi}{3P_p}\right)\right) & \sin\left(P_c\left(\theta_r - \alpha - \frac{4\pi}{3P_p}\right)\right) \\ \sqrt{\frac{1}{2}} & \sqrt{\frac{1}{2}} & \sqrt{\frac{1}{2}} \end{bmatrix} \quad (4\text{-}4)$$

4.2. Rotor Transformation

The rotor transformation is the translation of the electrical effects of the axes of the nests onto the dq axes. Since the rotor reference frame is used, there is no relative rotor-stator angle in the rotor transformation process. Each loop is transformed to equivalents on the dq axes by translating the mechanical displacement angle to the equivalent electrical angle through multiplication by the pole pairs of the winding. Each particular loop set of the same number within the nests is separately translated. Assembling the rotor transformation as a row matrix has the effect of summing the effects of all loops on an axis into a single equivalent combined loop. Each of the rotor loop transformations in (4-5)and (4-6) are identical; the subscripts are used only for consistency with the rotor impedance matrices.

$$\mathbf{C}_{rp} = \begin{bmatrix} \mathbf{C}_{rp1} & \mathbf{C}_{rp2} & \cdots & \mathbf{C}_{rpm} \end{bmatrix} \quad (4\text{-}5)$$

$$\mathbf{C}_{rc} = \begin{bmatrix} \mathbf{C}_{rc1} & \mathbf{C}_{rc2} & \cdots & \mathbf{C}_{rcm} \end{bmatrix} \quad (4\text{-}6)$$

Without loss of generality, the axis of the first nest is assumed aligned to the q-axis of the reference frame. The rotor loop transformation matrices, (4-7) and (4-8), are

rectangular since zero sequence currents cannot exist within the closed rotor and the n nests are to be reduced to two equivalent coils. The argument of the sinusoid functions is assumed negative since the reference frame is assumed stationary when viewed from the rotor. This is consistent with the development of the stator transformation matrices.

$$\mathbf{C}_{rpi} = \sqrt{\frac{2}{mn}}\begin{bmatrix} 1 & \cos\left(-P_p\frac{2\pi}{n}\right) & \cdots & \cos\left(-P_p\frac{2\pi}{n}(n-1)\right) \\ 0 & \sin\left(-P_p\frac{2\pi}{n}\right) & \cdots & \sin\left(-P_p\frac{2\pi}{n}(n-1)\right) \end{bmatrix} \tag{4-7}$$

$$\mathbf{C}_{rci} = \sqrt{\frac{2}{mn}}\begin{bmatrix} 1 & \cos\left(-P_c\frac{2\pi}{n}\right) & \cdots & \cos\left(-P_c\frac{2\pi}{n}(n-1)\right) \\ 0 & \sin\left(-P_c\frac{2\pi}{n}\right) & \cdots & \sin\left(-P_c\frac{2\pi}{n}(n-1)\right) \end{bmatrix} \tag{4-8}$$

Using the transformation matrices developed, the dq model can now be developed through the proper transformation of the impedances.

5. FORMULATION OF THE DQ MODEL

Using the abc to dq variable transformation relationship, (4-2), the voltage equation, (3-1), can be arranged as the rotor transformation product, (5-1), where all voltages are now assumed to be dq reference frame voltages.

$$\begin{bmatrix} \mathbf{v}_p \\ \mathbf{v}_c \\ \mathbf{v}_r \end{bmatrix} = \begin{bmatrix} \mathbf{C}_{sp} & \mathbf{0} & \mathbf{0} \\ \mathbf{0} & \mathbf{C}_{sc} & \mathbf{0} \\ \mathbf{0} & \mathbf{0} & \mathbf{C}_r \end{bmatrix} \begin{bmatrix} \mathbf{Z}_{sp} & \mathbf{0} & \mathbf{Z}_{spr} \\ \mathbf{0} & \mathbf{Z}_{sc} & \mathbf{Z}_{scr} \\ \mathbf{Z}_{spr}^T & \mathbf{Z}_{scr}^T & \mathbf{Z}_r \end{bmatrix} \begin{bmatrix} \mathbf{C}_{sp}^T & \mathbf{0} & \mathbf{0} \\ \mathbf{0} & \mathbf{C}_{sc}^T & \mathbf{0} \\ \mathbf{0} & \mathbf{0} & \mathbf{C}_r^T \end{bmatrix} \begin{bmatrix} \mathbf{i}_p \\ \mathbf{i}_c \\ \mathbf{i}_r \end{bmatrix} \tag{5-1}$$

However, there are two rotor transformation matrices which necessitates the splitting of the rotor currents and voltages into two components. One of the components is due to the interaction with the power winding, the other with the control winding. This will introduce two additional states, (5-2), which will later be combined.

$$\mathbf{v}_r = \begin{bmatrix} \mathbf{v}_{rp} \\ \mathbf{v}_{rc} \end{bmatrix}$$
$$\mathbf{i}_r = \begin{bmatrix} \mathbf{i}_{rp} \\ \mathbf{i}_{rc} \end{bmatrix} \tag{5-2}$$

The complete rotor transformation product to be calculated is now shown as (5-3). The states introduced into the rotor obey the law of superposition. Each of the voltages and currents have both q and d-axis components. The rotor will not support zero sequence terms. The stator quantities, however, may contain a zero sequence quantity if supplied from an unbalanced source.

$$\begin{bmatrix} \mathbf{v}_p \\ \mathbf{v}_c \\ \mathbf{v}_{rp} \\ \mathbf{v}_{rc} \end{bmatrix} = \begin{bmatrix} \mathbf{C}_{sp} & \mathbf{0} & \mathbf{0} & \mathbf{0} \\ \mathbf{0} & \mathbf{C}_{sc} & \mathbf{0} & \mathbf{0} \\ \mathbf{0} & \mathbf{0} & \mathbf{C}_{rp} & \mathbf{0} \\ \mathbf{0} & \mathbf{0} & \mathbf{0} & \mathbf{C}_{rc} \end{bmatrix} \begin{bmatrix} \mathbf{Z}_{sp} & \mathbf{0} & \mathbf{Z}_{spr} & \mathbf{Z}_{spr} \\ \mathbf{0} & \mathbf{Z}_{sc} & \mathbf{Z}_{scr} & \mathbf{Z}_{scr} \\ \mathbf{Z}_{spr}^{T} & \mathbf{0} & \mathbf{Z}_{r} & \mathbf{0} \\ \mathbf{0} & \mathbf{Z}_{scr}^{T} & \mathbf{0} & \mathbf{Z}_{r} \end{bmatrix} \begin{bmatrix} \mathbf{C}_{sp}^{T} & \mathbf{0} & \mathbf{0} & \mathbf{0} \\ \mathbf{0} & \mathbf{C}_{sc}^{T} & \mathbf{0} & \mathbf{0} \\ \mathbf{0} & \mathbf{0} & \mathbf{C}_{rp}^{T} & \mathbf{0} \\ \mathbf{0} & \mathbf{0} & \mathbf{0} & \mathbf{C}_{rc}^{T} \end{bmatrix} \begin{bmatrix} \mathbf{i}_p \\ \mathbf{i}_c \\ \mathbf{i}_{rp} \\ \mathbf{i}_{rc} \end{bmatrix} \quad (5\text{-}3)$$

The impedance terms in (5-3) contain the differential operators which operate on the product of inductance and current. This will introduce speed induced voltage terms, referred to as speed voltages, due to the differentiation of the sinusoid functions in the stator transformation matrices. The transformed dq impedance, $\mathbf{Z_{qd}}$, can be broken into a term that is not a function of the rotor angle, and one that is. Hence,

$$\mathbf{Z}_{qd}(r, L, \theta_r) = \mathbf{G}(r, L) + \mathbf{H}(L, \theta_r) \quad (5\text{-}4)$$

where r, L, and θ_r are the respective resistances, inductances, and rotor angles in the original impedance matrices. The sum, (5-4), can be expanded into the different matrices that need to be evaluated as shown below.

$$\mathbf{Z}_{qd} = \begin{bmatrix} \mathbf{g}_{11} & \mathbf{0} & \mathbf{g}_{13} & \mathbf{g}_{14} \\ \mathbf{0} & \mathbf{g}_{22} & \mathbf{g}_{23} & \mathbf{g}_{24} \\ \mathbf{g}_{31} & \mathbf{0} & \mathbf{g}_{33} & \mathbf{0} \\ \mathbf{0} & \mathbf{g}_{42} & \mathbf{0} & \mathbf{g}_{44} \end{bmatrix} + \begin{bmatrix} \mathbf{h}_{11} & \mathbf{0} & \mathbf{h}_{13} & \mathbf{h}_{14} \\ \mathbf{0} & \mathbf{h}_{22} & \mathbf{h}_{23} & \mathbf{h}_{24} \\ \mathbf{h}_{31} & \mathbf{0} & \mathbf{0} & \mathbf{0} \\ \mathbf{0} & \mathbf{h}_{42} & \mathbf{0} & \mathbf{0} \end{bmatrix} \quad (5\text{-}5)$$

From (5-5), the varying matrices can be classified as stator self impedance, mutual impedance, and rotor equations. The subsequent sections derive each of these equations. The trigonometric relationships in Appendix A are used to simplify the evaluation of the terms in (5-5).

5.1. Stator Self Impedance Matrix Equations

The power winding self impedance matrix equations involve two terms, one of which is a speed voltage term. The first product, $\mathbf{g_{11}}$, is defined as

$$\mathbf{g}_{11} = \mathbf{C}_{sp}\mathbf{Z}_{sp}\mathbf{C}_{sp}^{T}. \tag{5-6}$$

Using the angle relationships in Appendix A,

$$\mathbf{g}_{11} = \begin{bmatrix} r_p + L_p D_t & 0 & 0 \\ 0 & r_p + L_p D_t & 0 \\ 0 & 0 & r_p + L_{lp} D_t \end{bmatrix}, \quad L_p = \frac{3}{2} L_{mp} + L_{lp}. \tag{5-7}$$

Note that the resistances and leakage inductances of the windings are unaffected by the transformation process.

When computing the speed voltage terms of the power winding, the derivatives of the inductance-transformation matrix product must be taken. The resistances in the impedance matrix have been removed so that only inductances remain. The first speed voltage matrix to be solved, $\mathbf{h_{11}}$, is shown below, where $\mathbf{U_3}$ is the identity matrix of order 3.

$$\mathbf{h}_{11} = \mathbf{C}_{sp} D_t \left(\left(\mathbf{Z}_{sp} - r_p \mathbf{U}_3 \right) \mathbf{C}_{sp}^{T} \right) \tag{5-8}$$

Simplifying,

$$\mathbf{h}_{11} = P_p \omega_r L_p \begin{bmatrix} 0 & 1 & 0 \\ -1 & 0 & 0 \\ 0 & 0 & 0 \end{bmatrix} \tag{5-9}$$

where ω_r is the result of differentiating the rotor position.

The control winding equations, derived similarly, are as shown below.

$$\mathbf{g}_{22} = \begin{bmatrix} r_c + L_c D_t & 0 & 0 \\ 0 & r_c + L_c D_t & 0 \\ 0 & 0 & r_c + L_{lc} D_t \end{bmatrix}, \quad L_c = \frac{3}{2} L_{mc} + L_{lc} \tag{5-10}$$

and

$$\mathbf{h}_{22} = P_c \omega_r L_c \begin{bmatrix} 0 & 1 & 0 \\ -1 & 0 & 0 \\ 0 & 0 & 0 \end{bmatrix} \tag{5-11}$$

5.2. Mutual Impedance Matrix Equations

The matrices that reflect the mutual impedance between the rotor and the stator are the vehicles of coupling that make the BDFM work. The rotor transformation matrices, (4-5) and (4-6), do not depend upon the rotor position. Therefore, the differential operator acts only on the time varying inductance-current product and not on the transformation product. Note that, even though written as an impedance, the mutual impedance matrices are purely inductive. Begin by defining the following products,

$$\begin{aligned} \mathbf{g}_{13} &= \mathbf{C}_{sp} \mathbf{Z}_{spr} \mathbf{C}_{rp}^{\mathrm{T}} \\ \mathbf{h}_{13} &= \mathbf{C}_{sp} D_t \left(\mathbf{Z}_{spr} \right) \mathbf{C}_{rp}^{\mathrm{T}} \end{aligned} . \tag{5-12}$$

Simplifying (5-12) using the series expressions given in Appendix A, yields.

$$\mathbf{g}_{13} = M_p \begin{bmatrix} 1 & 0 \\ 0 & 1 \\ 0 & 0 \end{bmatrix} D_t, \quad \mathbf{h}_{13} = P_p \omega_r M_p \begin{bmatrix} 0 & 1 \\ -1 & 0 \\ 0 & 0 \end{bmatrix} \tag{5-13}$$

where

$$M_p = \left(\frac{n}{2}\right)\sqrt{\frac{3}{mn}}\sum_{j=1}^{m} M_{sprj}, \quad n = P_p + P_c. \tag{5-14}$$

Since $\mathbf{Z_{spr}}$ and the rotor transformation matrix, (4-5), are row matrices, the product has the effect of summing all of the magnitudes of each of the matrices to arrive at an equivalent dq mutual inductance between the power winding and the rotor, expressed as a closed form series as shown in (5-14).

Similarly, the value of $\mathbf{g_{14}}$ and $\mathbf{h_{14}}$ can be found. However, in this case, the control winding rotor transformation matrix, (4-6), is used as the right multiplying matrix. This results in a change of signs in the value of the matrices because the control winding transformation matrix is used to transform power winding mutual impedances as shown below.

$$\mathbf{g}_{14} = M_p \begin{bmatrix} 1 & 0 \\ 0 & -1 \\ 0 & 0 \end{bmatrix} D_t, \quad \mathbf{h}_{14} = P_p \omega_r M_p \begin{bmatrix} 0 & -1 \\ -1 & 0 \\ 0 & 0 \end{bmatrix} \tag{5-15}$$

Similar results are obtained when solving for the control winding dq mutual inductances. Transforming the impedances derived for one winding with the transformation derived for the other winding results in the effects each winding has on the other through the rotor. Without any intermediate steps, the results for the control winding mutual impedance matrices are shown below.

$$\mathbf{g}_{23}+\mathbf{h}_{23}=\begin{bmatrix} M_c D_t & -P_c\omega_r M_c \\ -P_c\omega_r M_c & -M_c D_t \\ 0 & 0 \end{bmatrix}$$
$$\mathbf{g}_{24}+\mathbf{h}_{24}=\begin{bmatrix} M_c D_t & P_c\omega_r M_c \\ -P_c\omega_r M_c & M_c D_t \\ 0 & 0 \end{bmatrix} \tag{5-16}$$

where

$$M_c=\left(\frac{n}{2}\right)\sqrt{\frac{3}{mn}}\sum_{j=1}^{m}M_{scrj}, \quad n=P_p+P_c \tag{5-17}$$

Elements $\mathbf{g_{31}}$ and $\mathbf{g_{42}}$ are the transpose of $\mathbf{g_{13}}$ and $\mathbf{g_{24}}$, respectively. However, the speed voltage terms, $\mathbf{h_{31}}$ and $\mathbf{h_{42}}$, when evaluated, are equal to zero. This results in no speed voltages induced into the rotor. This is to be expected since the motor is being modeled in the rotor reference frame.

5.3. Rotor Equations

The transformation of the rotor impedances results in an equivalent rotor inductance and resistance. The entire rotor transformation process for the power winding is described in the following equation:

$$\mathbf{g}_{33}=\mathbf{C}_{rp}\mathbf{Z}_r\mathbf{C}_{rp}^{T} \tag{5-18}$$

This product can be expanded so that

$$\mathbf{g}_{33}=\begin{bmatrix}\mathbf{C}_{rp1} & \mathbf{C}_{rp2} & \cdots & \mathbf{C}_{rpm}\end{bmatrix}\begin{bmatrix}\mathbf{Z}_{11} & \mathbf{Z}_{12} & \cdots & \mathbf{Z}_{1m}\\ \mathbf{Z}_{21} & \mathbf{Z}_{22} & \cdots & \mathbf{Z}_{2m}\\ \vdots & \vdots & \ddots & \vdots\\ \mathbf{Z}_{m1} & \mathbf{Z}_{m2} & \cdots & \mathbf{Z}_{mm}\end{bmatrix}\begin{bmatrix}\mathbf{C}_{rp1}^{T}\\ \mathbf{C}_{rp2}^{T}\\ \vdots\\ \mathbf{C}_{rpm}^{T}\end{bmatrix}. \tag{5-19}$$

The transformation of the terms in (5-19) is straightforward except for the transformation of the outer loop system impedance, $\mathbf{Z_{11}}$, when a caged rotor is used because of the presence of the common bar impedances of the outer loops. For a caged rotor, this transformation results in the following.

$$\mathbf{C}_{rp1}\mathbf{Z}_{11}\mathbf{C}_{rp1}^{T}=\frac{1}{m}\begin{bmatrix}r_{11}+(L_{11}+M_{11})D_t-2(r_{11}^{'}+L_{11}^{'})\cos\left(-P_p\frac{2\pi}{n}\right)D_t & 0\\ 0 & r_{11}+(L_{11}+M_{11})D_t-2(r_{11}^{'}+L_{11}^{'})\cos\left(-P_p\frac{2\pi}{n}\right)D_t\end{bmatrix} \tag{5-20}$$

This result shows the effects of the common bar impedance that was not present in earlier analyses [8-10]. In these previous analyses, only the 3-1 machine was investigated for which the cosine terms in (5-20) do not appear. This effect is important since the performance of the BDFM is sensitive to the rotor inductance.

The remaining transformations are straightforward so the details will not be shown. The transformation results in the following:

$$\mathbf{g}_{33}=\mathbf{g}_{44}=\begin{bmatrix}r_r+L_rD_t & 0\\ 0 & r_r+L_rD_t\end{bmatrix} \tag{5-21}$$

where

$$L_r=\frac{1}{m}\left(\sum_{j=1}^{m}(L_{jj}+M_{jj})+\overbrace{\sum_{j=1}^{m}\sum_{i=1}^{m}(M_{ij}+M_{ij}^{'})}^{i\neq j}-2\cos\left(-P_p\frac{2\pi}{n}\right)L_{11}^{'}\right) \tag{5-22}$$

and

$$r_r = \frac{1}{m}\left(\sum_{j=1}^{m}\sum_{i=1}^{m} r_{ij} - 2\cos\left(-P_p\frac{2\pi}{n}\right)r_{11}^{\cdot}\right) \tag{5-23}$$

These equations show the equivalent dq rotor inductance and resistance as a summation of the abc values. The effects of all the loops have been condensed into an equivalent impedance present on each of the axes.

5.4. Complete Voltage Equation

A voltage model, below, using the results of the transformation product can now be assembled which incorporates the two additional rotor states previously defined in (5-2).

$$\begin{bmatrix} v_{qp} \\ v_{dp} \\ v_{0p} \\ v_{qc} \\ v_{dc} \\ v_{0c} \\ v_{qrp} \\ v_{drp} \\ v_{qrc} \\ v_{drc} \end{bmatrix} = \left[\begin{array}{ccc|ccc|cc|cc} r_p + L_p D_t & P_p\omega_r L_p & 0 & 0 & 0 & 0 & M_p D_t & P_p\omega_r M_p & M_p D_t & -P_p\omega_r M_p \\ -P_p\omega_r L_p & r_p + L_p D_t & 0 & 0 & 0 & 0 & -P_p\omega_r M_p & M_p D_t & -P_p\omega_r M_p & -M_p D_t \\ 0 & 0 & r_p + L_{lp} D_t & 0 & 0 & 0 & 0 & 0 & 0 & 0 \\ \hline 0 & 0 & 0 & r_c + L_c D_t & P_c\omega_r L_c & 0 & M_c D_t & -P_c\omega_r M_c & M_c D_t & P_c\omega_r M_c \\ 0 & 0 & 0 & -P_c\omega_r L_c & r_c + L_c D_t & 0 & -P_c\omega_r M_c & -M_c D_t & -P_c\omega_r M_c & M_c D_t \\ 0 & 0 & 0 & 0 & 0 & r_c + L_{lc} D_t & 0 & 0 & 0 & 0 \\ \hline M_p D_t & 0 & 0 & 0 & 0 & 0 & r_r + L_r D_t & 0 & 0 & 0 \\ 0 & M_p D_t & 0 & 0 & 0 & 0 & 0 & r_r + L_r D_t & 0 & 0 \\ \hline 0 & 0 & 0 & M_c D_t & 0 & 0 & 0 & 0 & r_r + L_r D_t & 0 \\ 0 & 0 & 0 & 0 & M_c D_t & 0 & 0 & 0 & 0 & r_r + L_r D_t \end{array}\right] \begin{bmatrix} i_{qp} \\ i_{dp} \\ i_{0p} \\ i_{qc} \\ i_{dc} \\ i_{0c} \\ i_{qrp} \\ i_{drp} \\ i_{qrc} \\ i_{drc} \end{bmatrix} \tag{5-24}$$

In order to simplify the system described by the above equation, the rotor states must be combined. This can be accomplished by looking at the transformation of the dq rotor currents to the abc domain. Superposition holds so that

$$\mathbf{i}_r = \mathbf{C}_{rp}^{T}\mathbf{i}_{rp} + \mathbf{C}_{rc}^{T}\mathbf{i}_{rc}. \tag{5-25}$$

Expanding yields,

$$\begin{bmatrix} i_{r(1,1)} \\ i_{r(1,2)} \\ \vdots \\ i_{r(m,n)} \end{bmatrix}_{mn,1} = \begin{bmatrix} 1 & 0 \\ \cos\theta & \sin\theta \\ \vdots & \vdots \\ \cos((n-1)\theta) & \sin((n-1)\theta) \end{bmatrix}_{mn,2} \begin{bmatrix} i_{qrp} \\ i_{drp} \end{bmatrix} + \begin{bmatrix} 1 & 0 \\ \cos\beta & \sin\beta \\ \vdots & \vdots \\ \cos((n-1)\beta) & \sin((n-1)\beta) \end{bmatrix}_{mn,2} \begin{bmatrix} i_{qrc} \\ i_{drc} \end{bmatrix} \tag{5-26}$$

where

$$\theta = -P_p \frac{2\pi}{n}, \quad \beta = -P_c \frac{2\pi}{n}. \tag{5-27}$$

The subscripts on the matrix elements designate the loop and nest numbers. The subscripts on the matrices designate their dimension.

The currents on the left hand side of the equation are the abc rotor currents. However, since the transformation matrix is rectangular, the system is over determined. Therefore, the abc currents are only equivalent currents. There will be multiple solutions; the value of the currents that exist in the rotor loops cannot be determined with this model. Nevertheless, equivalent currents are adequate to describing the performance of the machine. The only limitation is that no design decisions concerning the grading of the conductors can be made using these equivalent currents.

Because the system is over determined of rank 2, only two independent equations exist which describe the system. This fact will be used to combine the four dq-axis rotor currents into two equivalent dq-axis rotor currents. Expanding (5-25) results in the following relationship for the q-axis currents:

$$i_{qr} \equiv i_{r(1,1)} = i_{qrp} + i_{qrc}. \tag{5-28}$$

Expanding the second row of (5-26) results in

$$i_{r(1,2)} - \cos(\theta) i_{r(1,1)} = \sin(\theta) i_{drp} + \sin(\beta) i_{drc} \tag{5-29}$$

and, realizing that

$$\frac{\sin(\theta)}{\sin(\beta)} = -1, \tag{5-30}$$

yields

$$i_{dr} \equiv \frac{I_{r(1,2)} - \cos(\theta) I_{r(1,1)}}{\sin(\theta)} = i_{drp} - i_{drc}. \tag{5-31}$$

The additional rotor states, created earlier for the simplification of the analysis in order to adequately incorporate the effects of both windings on the rotor, can now be combined through the definitions in (5-28) and (5-31). The final form of the BDFM dq voltage equation is shown as (5-32).

$$\begin{bmatrix} v_{qp} \\ v_{dp} \\ v_{0p} \\ v_{qc} \\ v_{dc} \\ v_{0c} \\ 0 \\ 0 \end{bmatrix} = \begin{bmatrix} r_p + L_p D_t & P_p \omega_r L_p & 0 & 0 & 0 & 0 & M_p D_t & P_p \omega_r M_p \\ -P_p \omega_r L_p & r_p + L_p D_t & 0 & 0 & 0 & 0 & -P_p \omega_r M_p & M_p D_t \\ 0 & 0 & r_p + L_{lp} D_t & 0 & 0 & 0 & 0 & 0 \\ 0 & 0 & 0 & r_c + L_c D_t & P_c \omega_r L_c & 0 & M_c D_t & -P_c \omega_r M_c \\ 0 & 0 & 0 & -P_c \omega_r L_c & r_c + L_c D_t & 0 & -P_c \omega_r M_c & -M_c D_t \\ 0 & 0 & 0 & 0 & 0 & r_c + L_{lc} D_t & 0 & 0 \\ M_p D_t & 0 & 0 & M_c D_t & 0 & 0 & r_r + L_r D_t & 0 \\ 0 & M_p D_t & 0 & 0 & -M_c D_t & 0 & 0 & r_r + L_r D_t \end{bmatrix} \begin{bmatrix} i_{qp} \\ i_{dp} \\ i_{0p} \\ i_{qc} \\ i_{dc} \\ i_{0c} \\ i_{qr} \\ i_{dr} \end{bmatrix} \tag{5-32}$$

Since the voltages are the driving inputs, the resultant model is a voltage forced model. The dq voltages can be found by transforming the abc domain quantities using the stator transformation matrices as shown in (5-33).

$$\begin{bmatrix} v_{qp} \\ v_{dp} \\ v_{0p} \end{bmatrix} = \mathbf{C}_{sp} \begin{bmatrix} v_{Ap} \\ v_{Bp} \\ v_{Cp} \end{bmatrix}$$
$$\begin{bmatrix} v_{qc} \\ v_{dc} \\ v_{0c} \end{bmatrix} = \mathbf{C}_{sc} \begin{bmatrix} v_{Ac} \\ v_{Bc} \\ v_{Cc} \end{bmatrix} \tag{5-33}$$

5.5. Torque Equation

The torque equation is derived based on the assumption of a linear magnetic circuit so that the co-energy can be used instead of the energy of the magnetic system. Using the impedances, the rate of change of the impedances multiplied by the current will yield the equation for the torque. The torque equation, in conjunction with (5-32), will describe the entire electromechanical system of the BDFM. The electrical torque can be expressed in terms of the abc variables as shown below.

$$T_e = \mathbf{i}_s \frac{\partial}{\partial \theta_r} \mathbf{Z}_{sr} \mathbf{i}_r \tag{5-33}$$

Substituting for the dq quantities,

$$T_e = \mathbf{i}_{qd}^{T} \begin{bmatrix} \mathbf{C}_{sp} & \mathbf{0} \\ \mathbf{0} & \mathbf{C}_{sc} \end{bmatrix} \frac{\partial}{\partial \theta_r} \begin{bmatrix} \mathbf{Z}_{srp} & \mathbf{Z}_{srp} \\ \mathbf{Z}_{src} & \mathbf{Z}_{src} \end{bmatrix} \begin{bmatrix} \mathbf{C}_{rp}^{T} & \mathbf{0} \\ \mathbf{0} & \mathbf{C}_{rc}^{T} \end{bmatrix} \mathbf{i}_{qdr}. \tag{5-34}$$

Simplifying the above in conjunction with (5-28) and (5-31) yields the final dq electrical torque equation as shown:

$$T_e = P_p M_p \left(i_{qp} i_{dr} - i_{dp} i_{qr} \right) - P_c M_c \left(i_{qc} i_{dr} + i_{dc} i_{qr} \right). \tag{5-35}$$

The final torque equation relates the mechanical system to the electrical system within the BDFM. Incorporating the inertia and damping of the mechanical system results in the final torque equation,

$$J\frac{d^2\theta_r}{dt}+B\frac{d\theta_r}{dt}=T_e-T_l. \tag{5-36}$$

In order to simulate the dynamic performance of the BDFM, the voltage equation, (5-32), and the above torque equation are used.

5.6. Comparison With Previous Model

When compared to the previously derived model [8-10], three observations can be made. First, the model developed here is able to consider any pole pair combination. This greatly enhances the utility of this model, allowing predictions of performance for machines for specific applications and speed ranges prior to manufacture.

Second, this model has a dq mutual inductance between the control winding and the rotor which is the negative of that derived in the earlier analysis. This is due to the previous analysis working with a common winding stator. The common winding stator has the a-phase of the control winding offset by 220 degrees from the a-phase of the power winding. The previous work only used the 40 degree offset in simplifying the transformation product. This reverses the signs of the sine functions, leaving the cosine functions the same. When comparing the performance predictions, the result is irrelevant so long as the equations are consistent; both models predict the exact same results for 3/1 pole-pair machines. This would be expected since the aligning of the two windings within the stator should not be significant to the overall performance of the machine.

Finally, because of its lack of generality, the previous analysis did not arrive at the extra function that shows the special influence the rotor slot leakage inductance has on the equivalent dq rotor inductance. When analyzing the 3-1 pole pair machine, the effect of the additional slot leakage inductance term is null because of the argument of the cosine function in (5-20). Consequently, since the machine is sensitive to the rotor inductance, analyzing varying machines with other than the 3-1 stator pole pair combination would yield erroneous results

6. STEADY STATE MODEL

Dynamic models are very useful in determining the speed of response of a system and viewing the transient behavior of a motor. However, the steady state operating conditions of the BDFM are important also. In many applications, the necessary motor response can be very slow, of the order of seconds, so that the steady state operating point is very important in comparison with the dynamics of going from one operating state to another. This chapter will show the development of the BDFM steady state model.

6.1. Voltage Transformation

A synchronous, steady state model of the BDFM is desired. This model will be voltage forced, similar to the voltage forced dynamic model presented earlier. Balanced voltages are assumed applied. The voltage functions are transformed to the dq domain using the stator transformation matrices, (4-3) and (4-4). The power winding voltages will be assumed to have the following form:

$$\begin{bmatrix} v_{Ap} \\ v_{Bp} \\ v_{Cp} \end{bmatrix} = \hat{V}_p \begin{bmatrix} \cos(\omega_p t) \\ \cos\left(\omega_p t - \frac{2\pi}{3}\right) \\ \cos\left(\omega_p t - \frac{4\pi}{3}\right) \end{bmatrix}. \tag{6-1}$$

The power winding voltage is assumed to be positive sequence. The applied control voltage can be either positive or negative sequence. The control phase voltages are shown below where the upper sign is used for positive sequence and the lower sign for

negative sequence. In addition, there is assumed an arbitrary time zero phase displacement in the voltages.

$$\begin{bmatrix} v_{Ac} \\ v_{Bc} \\ v_{Cc} \end{bmatrix} = \hat{V}_c \begin{bmatrix} \cos(\omega_c t - \phi_{cp}) \\ \cos\left(\omega_c t \mp \frac{2\pi}{3} - \phi_{cp}\right) \\ \cos\left(\omega_c t \pm \frac{2\pi}{3} - \phi_{cp}\right) \end{bmatrix} \tag{6-2}$$

The voltages are now transformed to the dq domain using the relationship expressed in (4-2) and the transformation matrices (4-3) and (4-4). The power winding dq voltages are

$$v_p = \sqrt{\frac{3}{2}} \hat{V}_p \begin{bmatrix} \cos(P_p \omega_r t - \omega_p t) \\ \sin(P_p \omega_r t - \omega_p t) \end{bmatrix}. \tag{6-3}$$

Because this is steady state, the rotor position is linearly dependent on the rotational velocity of the rotor. There are no zero sequence terms because balanced voltages are assumed to be applied.

The control winding voltages have the same form. The two possible applied sequences are reflected in the signs associated with the angular velocity of the control winding. The transformed voltages are shown below.

$$v_c = \sqrt{\frac{3}{2}} \hat{V}_c \begin{bmatrix} \cos(P_c \omega_r t - \omega_c t + \Gamma^{\pm}) \\ \sin(P_c \omega_r t - \omega_c t + \Gamma^{\pm}) \end{bmatrix} \tag{6-4}$$

$$\Gamma^{+} = \phi_{cp} - P_c \alpha, \quad \Gamma^{-} = -\phi_{cp} - P_c \alpha$$

The control voltages are written in terms of one angle, Γ, that can take on one of two values depending on the phase sequence. This proves to be easier when analyzing the machine, leading to simplified equations when solving the steady state describing equations for an operating point. In general, knowing the components of Γ is not necessary in analyzing the machine since this angle cannot be measured directly.

The angle α is a physical angle that can be measured in the machine or extracted from the winding diagram as shown previously in Fig. 3-1. The angle ϕ_{cp} cannot be measured in the machine. It is a phase shift angle that only has physical significance in the rotor reference frame. The combined angle, Γ, proves to be very important in determining the operating point of the system. It is analogous to the electrical torque angle as used in describing the behavior of synchronous machines. In fact, plots of torque versus this angle show that, depending on the excitation level of the control winding and the speed of operation, the machine can meet a variety of load torques, both motoring and generating, by internally varying Γ, as will be shown later.

6.2. Frequency of Analysis

Once the voltage equations are derived, they must be transformed into the phasor domain. The cosine function, in accordance with standard practice, will be used as the basis for the transformation to the phasor domain as shown below. When analyzing phasors, the frequency variation term is dropped and only the phase angle is used to represent the phasor.

$$\cos(\omega t + \Psi) = \mathrm{Re}\left\{e^{j(\omega t+\Psi)}\right\} \tag{6-5}$$

In order to analyze separate systems in the phasor domain, the systems must all be at the same frequency. Therefore, from (6-3) and (6-4), the following frequency relationship must hold in order that the machine be analyzed in the phasor domain.

$$\left(P_c\omega_r \mp \omega_c\right) = \pm\left(P_p\omega_r - \omega_p\right) \tag{6-6}$$

This analysis considers only machines with nests equal to the sum of the pole-pairs. With this rotor structure, only the negative sign relationship on the right side of (6-6) will enable an average torque to be produced in both windings. For the machine to work, and for the model to accurately predict the performance of the machine, the windings must be able to produce an average torque. Solving for the rotor angular frequency results in (2-1).

The valid relationship of the frequencies is

$$\omega_R \equiv \left(P_c\omega_r \mp \omega_c\right) = \left(\omega_p - P_p\omega_r\right). \tag{6-7}$$

However, an equally valid representation is to use

$$\omega_R \equiv \left(\pm\omega_c - P_c\omega_r\right) = \left(P_p\omega_r - \omega_p\right) \tag{6-8}$$

where the negative sign is placed on the left side of the (6-6) instead of the right. This alternate frequency relationship gives rise to an alternative, but equivalent circuit. Only the form in (6-7) will be used for analysis since this form is more like the form analyzed previously for the 3-1 pole pair BDFM [4, 10] which will enable comparisons to be made more readily.

6.3. Steady State Voltage Model

The frequency of the phasors is given in (6-7). The voltage equations can be written in terms of complex phasor quantities as shown, where all voltages are assumed to be dq steady state voltages. Even though peak voltages are shown, rms quantities can be used so that the resulting circuit model is in terms of measurable quantities.

$$\begin{aligned} \mathbf{V_p} &= \sqrt{\frac{3}{2}}\hat{V}_p \begin{bmatrix} 1 \\ j \end{bmatrix} \\ \mathbf{V_c} &= \sqrt{\frac{3}{2}}\hat{V}_c \begin{bmatrix} e^{-j\Gamma^{\pm}} \\ je^{-j\Gamma^{\pm}} \end{bmatrix} \end{aligned} \tag{6-9}$$

The currents can be similarly defined. However, in defining the phase angles, it is assumed that all currents will, arbitrarily, have a positive phase angle. Even though the machine may not operate with positive current phase angles under all conditions, using such will simplify the analysis of the torque equation.

$$\begin{aligned} \mathbf{I_p} &= \sqrt{2}\tilde{I}_p \begin{bmatrix} e^{j\Phi_p} \\ je^{j\Phi_p} \end{bmatrix} \\ \mathbf{I_c} &= \sqrt{2}\tilde{I}_c \begin{bmatrix} e^{j\Phi_c^{\pm}} \\ -je^{j\Phi_c^{\pm}} \end{bmatrix} \end{aligned} \tag{6-10}$$

The current equation, above, is in terms of the rms currents, denoted by a tilde above the quantity, developed in the windings. The ± on the phase angle of the control winding current denotes whether the phase is for positive or negative sequence excitation, respectively. For analysis purposes, only the magnitude and sign of the total angle is important. Knowledge of the components that make up the angle is not useful in determining the machine's steady state operating point.

The rotor current needs to be defined with the same structure as the stator power winding currents in order that an average torque be produced. Under steady state conditions, it is essential that an average torque be produced for a valid synchronous model. Hence, the rotor current definition is

$$\mathbf{I}_r = \sqrt{2}\tilde{I}_r \begin{bmatrix} e^{j\phi_r} \\ je^{j\phi_r} \end{bmatrix} \tag{6-11}$$

The time derivatives of the currents are derived from (6-3) and (6-4) and are shown below.

$$\begin{aligned} D_t\mathbf{I}_p &= j(\omega_p - P_p\omega_r)\mathbf{I}_p \\ D_t\mathbf{I}_c &= j(P_c\omega_r \mp \omega_c)\mathbf{I}_c \\ D_t\mathbf{I}_r &= j\omega_R\mathbf{I}_r \end{aligned} \tag{6-12}$$

Equations (6-9) - (6-12) are now inserted into the dynamic voltage equation, (5-32). The q-axis voltage equations are used since, by definition, the q-axis is aligned with the a-phase axis of the power windings. All currents are written in terms of the q-axis currents to arrive at the customary system used for analysis. When the d-axis voltage equation is used and the currents are written in terms of the d-axis quantities, the d-axis model results. Making the substitutions, above, in the q-axis dynamic voltage equation results in the following steady state dq model where all quantities are rms values:

$$\begin{aligned} V_{qp} &= (r_p + j\omega_p L_p)I_{qp} + j\omega_p M_p I_{qr} \\ V_{qc} &= (r_c \mp j\omega_c L_c)I_{qc} \mp j\omega_c M_c I_{qr} \\ V_{qr} &= r_r I_{qr} + j\omega_R(L_r I_{qr} + M_p I_{qp} + M_c I_{qc}) = 0 \end{aligned} \tag{6-13}$$

These equations lend themselves to the equivalent circuit model shown. Note the use of current controlled voltage sources in the model. This is the most accurate representation of the voltage equations since it accounts for the variation in the self impedance of the control winding.

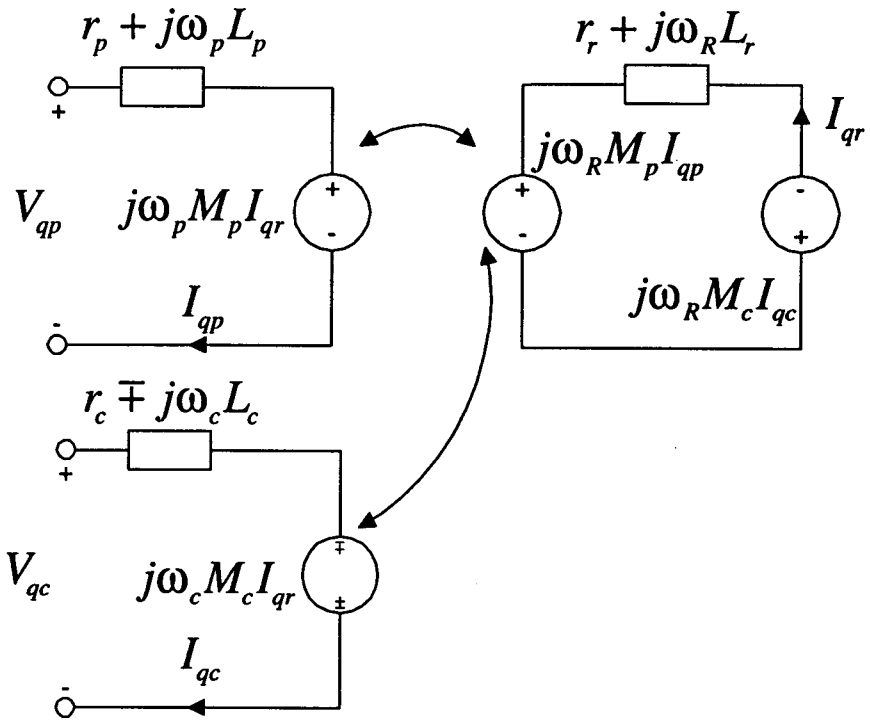

Figure 6-1. Steady state equivalent circuit

An interesting result of the model is that the control winding has a negative self inductance when under positive sequence excitation. This is due to analysis in the rotor reference frame. If the alternate frequency convention defined in (6-8) were used, the negative self reactance would be seen in the power winding. In addition, the signs on the frequency elements of the control winding voltage expression would be reversed. Either model is representative of the performance of the machine.

The steady state model is only valid when the BDFM is synchronized. There must be induced voltages in all circuits in order for the model to be valid. For example, the model is not valid if there is no control winding current; the motor could not possibly be synchronized under this situation. However, the model can accept any frequency of excitation on either winding, e.g. dc on the control winding given by $\omega_c = 0$.

For the sake of completeness, the d-axis equations are derived similarly to the q-axis currents. In this case, the d-axis dynamic voltage equations are used. All equations are written in terms of the d-axis quantities through the use of the *j* operator, as applicable. The d-axis equations, without derivation, are shown below.

$$\begin{aligned} V_{dp} &= (r_p + j\omega_p L_p) I_{dp} + j\omega_p M_p I_{dr} \\ V_{dc} &= (r_c \mp j\omega_c L_c) I_{dc} \pm j\omega_c M_c I_{dr} \\ V_{dr} &= r_r I_{dr} + j\omega_R (L_r I_{dr} + M_p I_{dp} - M_c I_{dc}) = 0 \end{aligned} \tag{6-14}$$

In comparison with the synchronous model developed in [8, 10], this model avoids the use and definition of slips. Using slips can be confusing since the term slip implies asynchronous operation whereas this model is for synchronous operation. In addition, the use of slip in the control voltage equation in [4, 8, 10] precluded analysis with dc excitation of the control model without defining a separate, dc excited model. The model presented here handles all applied frequencies equally well.

6.4. Torque Equation

In order to incorporate the mechanical influence on the BDFM, the electrical torque equation must be written in terms of the steady state currents. In order to derive

the steady state torque equation, the time varying, sinusoidal dq currents are substituted in (5-35) with the following result:

$$T_e = 2P_pM_p\tilde{I}_p\tilde{I}_r\sin(\phi_p-\phi_r)-2P_cM_c\tilde{I}_c\tilde{I}_r\sin(\phi_c-\phi_r) \tag{6-14}$$

where the currents are rms quantities. The factor of two shows that either axis of the steady state winding model, i.e. d or q, can be used to sufficiently describe the system. By using the following trigonometric identity,

$$\sin(x-y)=\sin x\cos y-\cos x\sin y \tag{6-15}$$

and the fact that the phase angles can be related to the complex components of the currents, the following simplified torque equation, suitable for simulation purposes, results.

$$\begin{aligned} T_e = {} & 2P_pM_p\left(\mathrm{Im}\{I_{qp}\}\mathrm{Re}\{I_{qr}\}-\mathrm{Re}\{I_{qp}\}\mathrm{Im}\{I_{qr}\}\right) \\ & -2P_cM_c\left(\mathrm{Im}\{I_{qc}\}\mathrm{Re}\{I_{qr}\}-\mathrm{Re}\{I_{qr}\}\mathrm{Im}\{I_{qr}\}\right) \end{aligned} \tag{6-16}$$

6.5. Steady State Simulation Model

The steady state model can be broken into real and imaginary components, similar to the torque equation, in order to predict the steady state performance of the BDFM. The real and imaginary parts of the system become the states of the electrical system. In addition to the currents, the phase angle between the power winding voltage and control winding voltage is a state. The combinations of these elements yields a seventh order

system. The six current equations, both real and imaginary parts, and the torque equation completely describe the steady state performance of the BDFM. Assign states as follows:

$$\begin{aligned}&\begin{bmatrix} x_1 & x_2 & x_3 & x_4 & x_5 & x_6 & x_7 \end{bmatrix}^T = \\ &\begin{bmatrix} \mathrm{Re}\{I_{qp}\} & \mathrm{Im}\{I_{qp}\} & \mathrm{Re}\{I_{qc}\} & \mathrm{Im}\{I_{qc}\} & \mathrm{Re}\{I_{qr}\} & \mathrm{Im}\{I_{qr}\} & \Gamma^{\pm} \end{bmatrix}^T.\end{aligned} \tag{6-17}$$

The describing voltage equation is shown below.

$$\begin{bmatrix} \frac{\sqrt{3}}{2}\hat{V}_p \\ 0 \\ \frac{\sqrt{3}}{2}\hat{V}_c\cos(x_7) \\ \frac{\sqrt{3}}{2}\hat{V}_c\sin(x_7) \\ 0 \\ 0 \end{bmatrix} = \begin{bmatrix} r_p & -\omega_p L_p & 0 & 0 & 0 & -\omega_p M_p \\ \omega_p L_p & r_p & 0 & 0 & \omega_p M_p & 0 \\ 0 & 0 & r_c & \pm\omega_c L_c & 0 & \pm\omega_c M_c \\ 0 & 0 & \mp\omega_c L_c & r_c & \mp\omega_c M_c & 0 \\ 0 & -\omega_R M_p & 0 & -\omega_R M_c & r_r & -\omega_R L_r \\ \omega_R M_p & 0 & \omega_R M_c & 0 & \omega_R L_r & r_r \end{bmatrix} \begin{bmatrix} x_1 \\ x_2 \\ x_3 \\ x_4 \\ x_5 \\ x_6 \end{bmatrix} \tag{6-18}$$

Coupled with the torque equation, the states of the system can be found. Even though (6-18) is linear, introducing the torque equation results in a non-linear system. The states of the system must be found by an iterative process. The Newton-Raphson root finding technique has proven to be satisfactory, provided an adequate initial guess of Γ can be found so that the system converges to a valid operating point.

In order to use the Newton-Raphson technique, the describing equations must be placed in a form suitable to root finding. In addition, the Jacobian of the system of equations must also be determined. The Newton-Raphson root solving technique is described by the following equations.

$$\mathbf{x}_i^{new} = \mathbf{x}_i^{old} + \delta\mathbf{x}_i$$
$$\delta\mathbf{x}_i = -\left(\frac{\partial \mathbf{F}}{\partial \mathbf{x}}\right)^{-1}\mathbf{F} \tag{6-19}$$

The functions to be solved are as given below.

$$\mathbf{F} = \begin{bmatrix} r_p x_1 - \omega_p L_p x_2 - \omega_p M_p x_6 - \frac{\sqrt{3}}{2}\hat{V}_p \\ \omega_p L_p x_1 + r_p x_2 + \omega_p M_p x_5 \\ r_c x_3 \pm \omega_c L_c x_4 \pm \omega_c M_c x_6 - \frac{\sqrt{3}}{2}\hat{V}_c \cos(x_7) \\ \mp\omega_c L_c x_3 + r_c x_4 \mp \omega_c M_c x_5 - \frac{\sqrt{3}}{2}\hat{V}_c \sin(x_7) \\ -\omega_R M_p x_2 - \omega_R M_c x_4 + r_r x_5 - \omega_R L_r x_6 \\ \omega_R M_p x_1 + \omega_R M_c x_3 + \omega_R L_r x_5 + r_r x_6 \\ 2P_p M_p (x_2 x_5 - x_1 x_6) - 2P_c M_c (x_4 x_5 - x_3 x_6) \end{bmatrix} = \mathbf{0} \tag{6-20}$$

The corresponding Jacobian is as follows:

$$\frac{\partial \mathbf{F}}{\partial \mathbf{x}} = \begin{bmatrix} r_p & -\omega_p L_p & 0 & 0 & 0 & -\omega_p M_p & 0 \\ \omega_p L_p & r_p & 0 & 0 & \omega_p M_p & 0 & 0 \\ 0 & 0 & r_c & \pm\omega_c L_c & 0 & \pm\omega_c M_c & \frac{\sqrt{3}}{2}\hat{V}_c \sin(x_7) \\ 0 & 0 & \mp\omega_c L_c & r_c & \mp\omega_c M_c & 0 & -\frac{\sqrt{3}}{2}\hat{V}_c \cos(x_7) \\ 0 & -\omega_R M_p & 0 & -\omega_R M_c & r_r & -\omega_R L_r & 0 \\ \omega_R M_p & 0 & \omega_R M_c & 0 & \omega_R L_r & r_r & 0 \\ -2P_p M_p x_6 & 2P_p M_p x_5 & 2P_c M_c x_6 & -2P_c M_c x_5 & 2P_p M_p x_2 - 2P_c M_c x_4 & -2P_p M_p x_1 + 2P_c M_c x_3 & 0 \end{bmatrix} \tag{6-21}$$

The functions and their Jacobian are used to find the steady state operating point of the system. The root finding method needs an initial guess of the states. The

conceptual angle between the two voltages, Γ, is guessed. This is used to solve for the initial currents by inverting the impedance matrix depicted in (6-18) and multiplying by the corresponding voltage vector. The initial currents are used as the old value of the state; the Jacobian is used to find the change of state. The system will normally converge to a reasonable level of accuracy within 30 iterations. This mathematical model can now be used to make performance predictions of any pole-pair combination machine.

7. MODEL VERIFICATION

The steady state BDFM model will be used to predict the performance of a 5 hp laboratory prototype BDFM. Comparisons will be made to measured data to show the validity of the model. Afterwards, the model will be used to predict the steady state performance of a 60 hp pump drive with both a 3/1 and a 4/2 stator pole pair geometry.

7.1. Steady State Predictions of the Lab Machine

The laboratory prototype is a BDFM constructed using a 5 hp standard induction motor frame. The control winding is excited through a series resonant current source inverter. Data were taken using the automated data acquisition system that involves various current, voltage, and power transducers. The layout of the lab is discussed further in [19].

The machine in the laboratory has been tested under a simulated pump load torque where the load torque is proportional to the square of the speed of the motor. The load torque varies from 13.8 Nm at 587 r/min to 31.5 Nm at 867 r/min. A pump load torque was chosen because the BDFM has a strong likelihood of finding a niche application in the pump drive market.

The measured values of speed, load torque, and stator voltages are input into the BDFM model and the values of the currents, power factors, and efficiency are calculated. The measured data for the BDFM is given in detail in [19]. The comparison of the predicted and measured stator currents for the laboratory BDFM prototype is shown in Fig. 7-1. There is a high correlation between the model and the predicted currents. The power winding current estimate is lower than the actual value, however, it is within an average error of 13%. This correlation suggests the model can be successfully used to predict the stator currents of future BDFM designs prior to manufacture. The parameters

for the BDFM used in the simulation were estimated using standard induction machine theory [13-17] and are as shown in Table 7-1. Discrepancies near 900 r/min can be expected since this speed corresponds to near 0 Hz frequency on the converter which is only approximated with the laboratory converter.

Table 7-1. 5 Hp BDFM DQ Model Parameters

Rp: 0.672 Ω	Rc: 0.924 Ω
Lp: 0.066496 H	Lc: 0.378444 H
Rr: 0.000164 Ω	Mp: 0.000839 H
Lr: 4.291706e-05 H	Mc: 0.003195 H

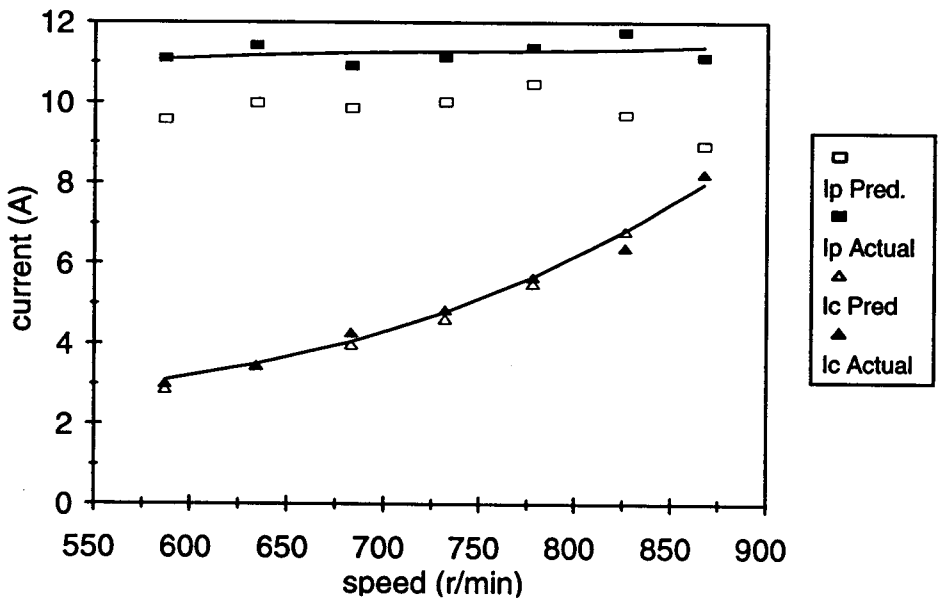

Figure 7-1. Stator currents of the 5 hp laboratory prototype BDFM

Comparison between the measured and predicted efficiency of the BDFM is shown in Fig. 7-2. The measured efficiency of the BDFM is lower than the predicted efficiency for several reasons. The current BDFM model includes neither the core loss nor the stray load loss of the machine. In addition, the measured efficiency includes the bearing loss, friction and windage losses, and the converter loss. The sum of these measured losses is presumed to explain the gap in predicted versus measured efficiency. Further refinements of the model will attempt to include the core loss of the machine which is, most probably, the highest of the previously mentioned losses.

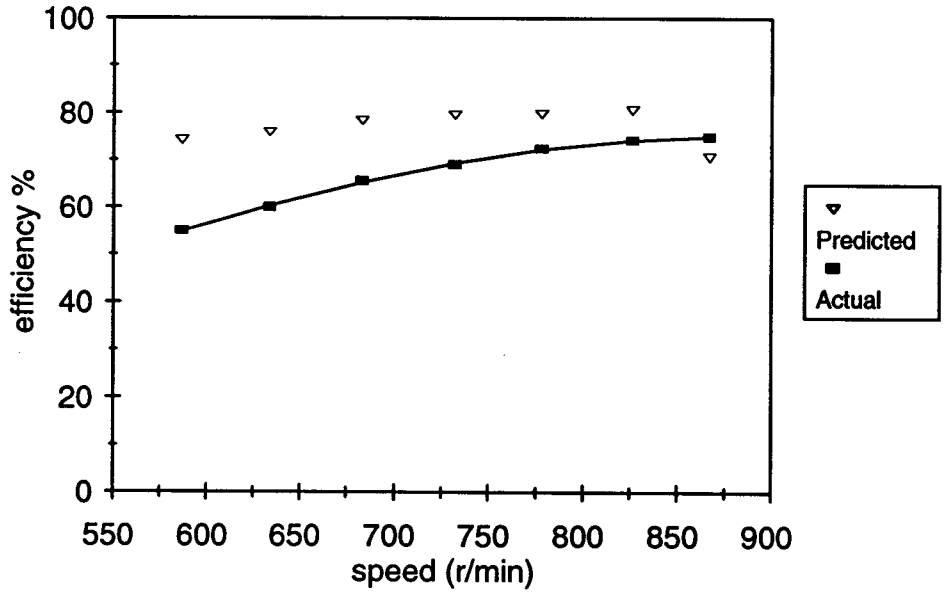

Figure 7-2. Comparison of measured and predicted efficiency for the 5 hp BDFM

Comparison of the measured and predicted power winding power, shown in 7-3, shows good correlation. The testing procedure did not try to maintain a certain power factor so the power factor is less than that obtainable with proper excitation on the control

winding. By changing the applied voltage level on the control winding, the power factor could have been changed to be either leading or unity instead of lagging.

Since the levels of currents are important in the rating of the motor and ancillary power electronics, the ability of the model to predict the current levels outweighs any over estimate of efficiency. Another reason for the differences in predicted and measured results is the existence of harmonics introduced into the motor by the thyristor, series resonant converter used to excite the control winding. The model assumes that the inputs are sinusoidal and that the winding distributions are ideal so that effects due to both time and space harmonics cannot be predicted. By including the core loss and other effects, the model will more closely predict the performance of the machine.

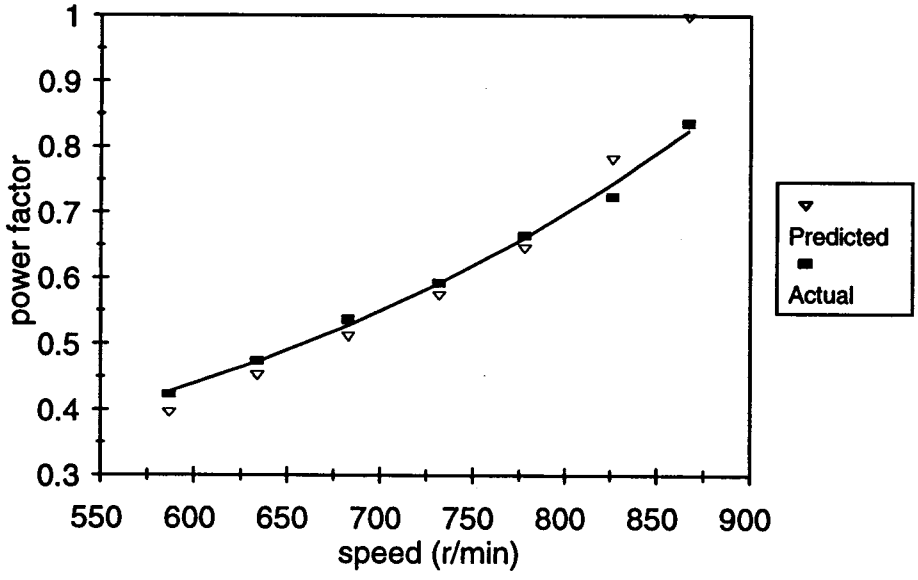

Figure 7-3. Comparison of measured and predicted power winding power factor for the 5 hp BDFM

7.2. BDFM Synchronous Operation

Using the steady state model, various information about the performance capabilities of the machine can be extracted. For instance, given a certain speed and voltage on the control winding, the maximum torque that can be produced by the machine can be estimated which is dependent on the value of the angle between the two stator voltages, Γ. Steady state analysis of the BDFM, depending on the excitation level of the control winding, shows two stable operating points. However, only one of the operating points is realizable; the other is only a result of the mathematical model and cannot be reached in practice.

Figure 7-4 shows the torque producing capability of the 5 hp laboratory BDFM at 600 r/min on a 230 V, 60 Hz supply with different values of control winding excitation. The steady state operating point is determined by the intersection of the load torque and the electrical torque. As can be seen, the control winding excitation level is critical for torque production. From Fig. 7-4, the torque capability of the motor for Vc = 10 V is low. For example, if the excitation were 10 V with no load torque applied, the motor will not synchronize because the electrical torque capability of the machine, at this excitation level, intersects the zero electrical torque point. This may not seem intuitive. However, it shows that the excitation must be greater than 10 V in order to synchronize the machine. Afterwards, the level may be reduced if the load torque does not exceed the torque maximums shown for that excitation level. Varying the excitation level changes the magnitude of each of the lobes of the curve.

Figure 7-5 shows that with Vc = 100 V, the motor will be able to remain in synchronism with a maximum motoring load torque of 38 Nm in contrast to only 14 Nm of generating torque. In addition, with the present level of excitation, this machine will never reach unity power factor since the imaginary current is always negative. In fact, this machine is operating with a leading power winding power factor.

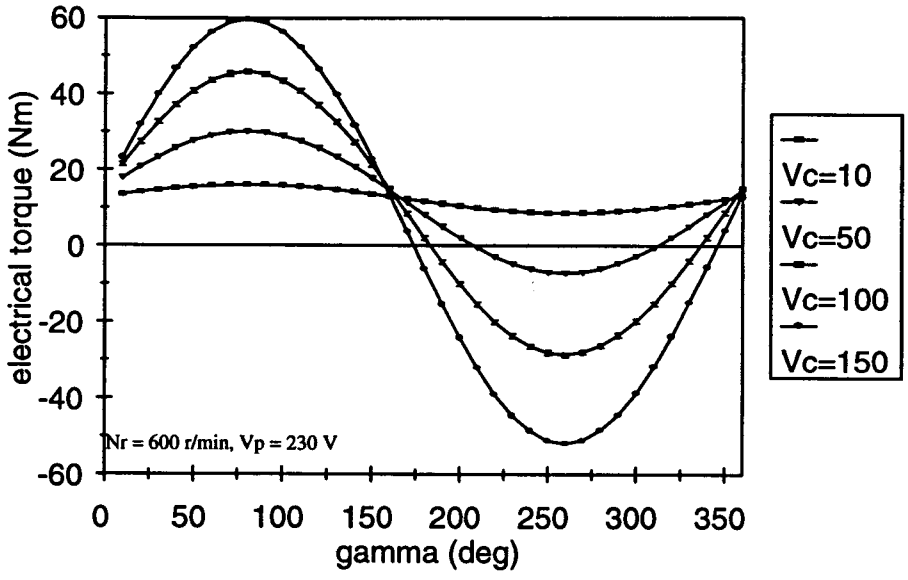

Figure 7-4. Torque vs. gamma for different excitation levels on the 5 hp BDFM

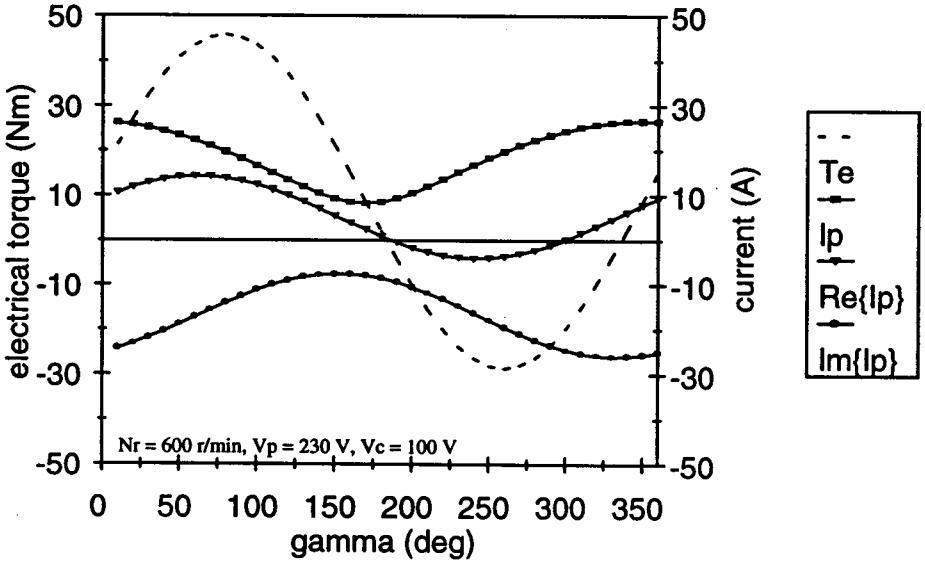

Figure 7-5. Electrical torque and power winding current vs. gamma for the 5 hp BDFM

Obviously, there will be two steady state operating points since the torque curve is not a single valued function. The realizable operating point is where the winding currents are at their minimum value for a given load torque. Normally, the location where the imaginary current is minimum will yield this operating point. For the data shown in Fig. 7-5, the valid operating points will occur for gamma between 85 and 265 deg. The angle where the minimum occurs is important for an initial guess on the electrical torque angle, Γ, needed to solve the non-linear steady state equations.

Figure 7-6 shows the control winding currents using the same speed and excitation voltage as in Fig. 7-5. Notice that when a generating torque is applied, the real part of the control winding current is negative which signifies generating current. Moreover, for this speed, a generating torque will result in both positive and negative real current in the power winding depending on the level of the generating torque as shown in Fig. 7-5. Since a generating torque does not always produce negative real power winding current, the motor would not be well suited to power generation at this speed and excitation level; it is more suitable as a motor for this operating condition.

Using this type of steady state analysis, the steady state model can establish operating limits and outline the capabilities of a particular BDFM design.

7.3. 60 Hp Pump Drive

Currently, a 3/1 60 hp BDFM is being constructed to replace an existing wound rotor induction machine that is being used in a municipal waste water treatment plant. The existing machine uses external resistors connected to the rotor to control the speed of the pump from 600-900 r/min. The analysis of the current system and the proposed design of a 3/1 BDFM to replace the existing drive is contained in [20-21]. Other pole-pair combination machines were not considered due to a lack of experience and design tools able to predict the performance of such a machine. The torque varies proportional to the

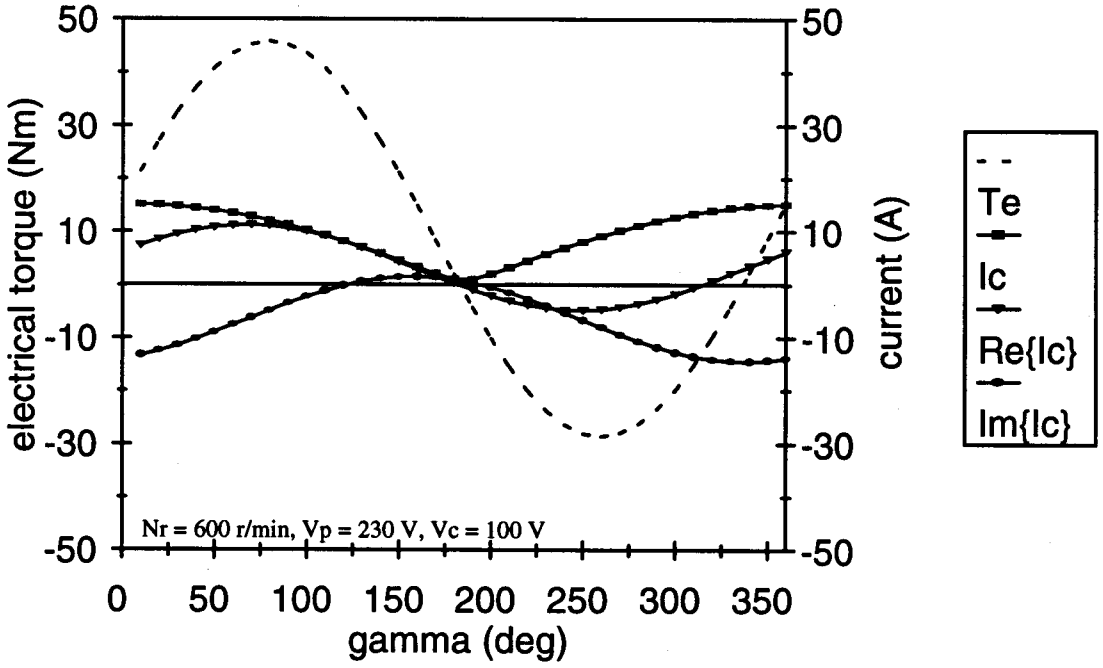

Figure 7-6. Electrical torque and control winding currents vs. gamma for the 5 hp BDFM

square of the speed with rated toque being 478 Nm at 900 r/min to 212 Nm at 600 r/min. The steady state model developed here now acts as the tool with which to analyze different pole-pair numbered machines. Using the general pole number model, alternative proposed BDFM designs can be considered.

One alternative design to the 3/1 BDFM pump drive is a 4/2 BDFM chosen for its good cross coupling factor [22] (As this paper is not generally available at this time, it is included in Appendix B.). The 4/2 design is a suitable replacement drive for the existing wound rotor induction machine provided the working top speed can be less than 900 r/min since this speed corresponds to the 60 Hz stator field speed of the 4 pole-pair winding where the machine will not be able to produce electrical torque. Use of the steady state model will determine how close this proposed BDFM can operate to the 900 r/min limit.

Figure Fig. 7-7 shows the torque capability of the 4/2 machine for different rotor speeds close to 900 r/min. The control winding and the supply voltages are 460 V. The rated torque of 478 Nm at 900 r/min is not obtainable for this machine. However, at 860 r/min the required load torque is 436 Nm, which is obtainable; the machine can support up to 861 Nm at this speed. Note that as the speed increases, the torque capability decreases rapidly as the 60 Hz stator field speed of the 8 pole winding is reached. The parameters used for the performance prediction are given in Table 7-2. Further analysis of the performance of the 4/2 machine is included in Appendix B.

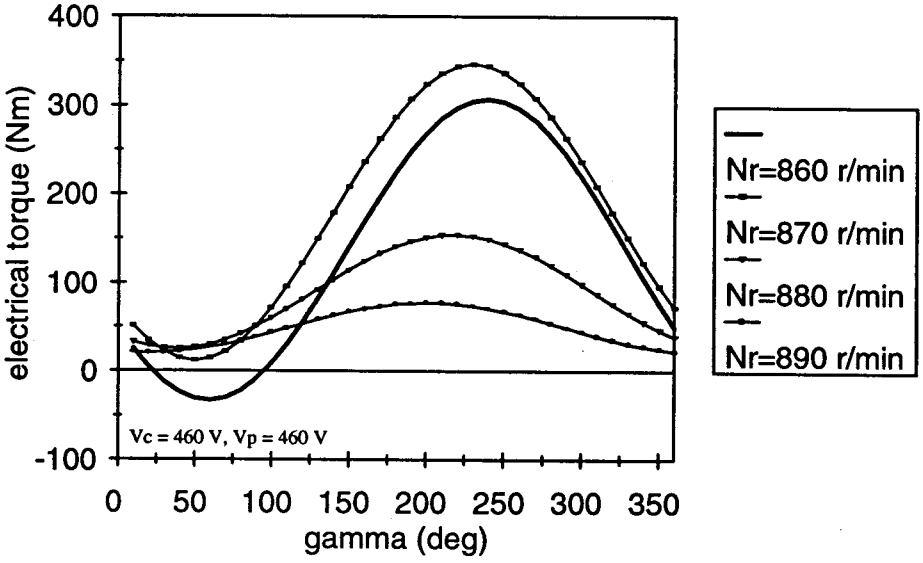

Figure 7-7. Electrical torque capability vs. gamma for different rotor speeds of the 4/2 60 hp BDFM

The 3/1 BDFM design originally proposed in [20-21] has been modified based on the results of the steady state simulations using this model. The number of turns per coil on the control winding has been lowered from eight to four. Ideally, the control winding excitation is adjusted to yield a near unity power winding power factor operation.

However, for the original design, the impedance of the control winding was so large that the voltage needed to obtain unity power factor operation exceeded the supply voltage. Lowering the turns per coil to four enables the machine to be operated through a greater speed range without reaching the limit of the supply.

Table 7-2. Parameters used in simulating the 4/2 BDFM

Rp: 0.13932 Ω	Rc: 0.60888 Ω
Lp: 0.034282 H	Lc: 0.435893 H
Rr: 0.000285 Ω	Mp: 0.000984 H
Lr: 8.615984e-05 H	Mc: 0.00467 H

Figure 7-8 shows the tradeoff associated with choosing the number of turns on the control winding, N_C. For the low number of turns, the machine is able to maintain unity power factor from approximately 700 to 900 r/min versus a range of 850 - 900 r/min for higher number of turns on the control winding. The reason for the inability of the 8 turns per coil control winding case to achieve unity power factor is that the voltage limits at line voltage at the high end of the speed range. The machine, in practice, is not normally operated at the low end of the speed range so that a reasonably low power factor is acceptable in that region. In addition, the ability of the machine to maintain near unity power factor operation may not be needed in this application due to the presence of power factor correction capacitors. Nevertheless, the model is able to illustrate the considerations for design of a BDFM.

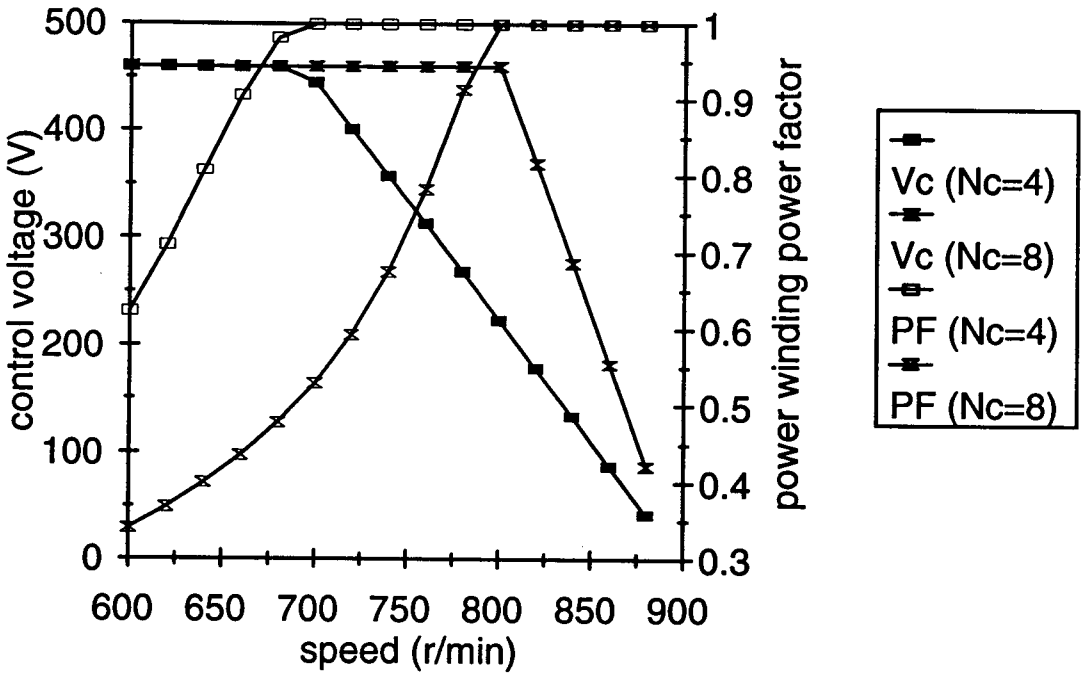

Figure 7-8. Control voltage and power winding power factor for the 3/1 60 hp BDFM pump drive

8. CONCLUSIONS

Adjustable speed drives and variable speed generators are being used more frequently in industry to increase a plant's efficiency. The BDFM is an alternative machine that has advantages over conventional induction motor drives in these applications. One of these advantages is the ability of the BDFM to control its power factor by varying the excitation of the control winding, similar to the adjusting of the field current on a synchronous machine. Different operating speed ranges demand the investigation of pole-pair numbered machines of other than the 3/1 BDFM. The lack of an adequate model has hampered these investigations until now.

The general pole number model of the BDFM that has been developed here is applicable to the analysis of any pole-numbered BDFM. First, the impedance equations that describe the interactions of the stator and the rotor of the machine were written. These impedance matrices were transformed into a two axis equivalent system that rotates with the rotor. The machine behavior is then readily understood through the interpretation of the equivalent circuit dynamic, or steady state synchronous model. Assumptions necessary made during the model development and their significance are outlined in Table 8-1.

The dynamic model should be suitable for prediction of the dynamic performance of the BDFM through the use of six electrical and one mechanical dynamic equations. In order to better understand the steady state synchronous operation of the BDFM, the steady state model was developed. The steady state model can be used to give insight into the load torque capabilities of the machine. For example, given an initial operating speed and control winding excitation, the amount of torque that the machine can produce, as well as the values of the currents, can be rapidly determined for any load condition. In addition, the existence of a synchronous operating condition can be readily determined given the speed and the control winding excitation.

Table 8-1. Assumptions made during model development

Assumption	Primary Effect
1. No direct coupling between the two stator winding systems.	Enables development of the impedance matrices.
2. The axes of each of the phases of the windings are assumed to be 120 electrical degrees apart	Simplifies development of the impedance matrices.
3. The rotor is non-salient.	Enables development of simplified impedance matrices.
4. Sinusoidal voltages are applied and the effects of other harmonics are ignored.	Allows simplified analysis in the dq domain.
5. Core loss and stray load loss are ignored.	Leads to over estimates of system efficiency.
6. The magnetic circuit is assumed to be linear.	Enables development of a simplified electrical torque equation.
7. The complete rotor transformation matrix is grouped as a row matrix.	Results in an equivalent rotor impedance at the expense of being able to extract the individual loop currents.

Correlation between data previously obtained for the 3/1 5 hp laboratory prototype and predictions from the model verifies the validity of the analysis. The model is able to accurately represent the currents. However, the efficiency prediction is optimistic. This is presumed to be caused by the model not considering losses other than the resistive I^2R

losses. In addition, the model considers neither time harmonics of the voltages and currents nor space harmonics of the winding distributions.

The general pole number model should eventually incorporate the core loss of the machine which is likely to be high due to the large currents induced in the rotor because of the high slips of the rotor with respect to each of the stator windings. Because the control winding will not normally be excited with pure sinusoids, the effects of harmonics should, eventually, be included when analyzing the machine performance. If fault studies are to be performed, the effects of unbalanced excitation should be incorporated into the model. This should be relatively easy and can be accomplished by including the zero sequence components of the voltages and using a refined equivalent circuit.

In conclusion, two axis reference frame theory has simplified the describing equations of the BDFM without the loss of analysis capabilities which resulted in a general pole number model in both dynamic and steady state form. This model has great utility in analyzing the various pole-pair combinations possible in a BDFM. It is very useful in examining the best choice of pole-pairs for a specific application. And, finally, the steady state synchronous capabilities can easily be determined given the operating speed and voltage level of the control winding.

REFERENCES

[1] Y. Liao and C. Sun, "A Low Cost, Robust Sensorless Controlled Scheme for Doubly-Fed Reluctance Motor Drives," *IEEE Industry Application Society Annual Meeting Conference Record*, pp. 437-44, 1993.

[2] Y. Xu and Y. Tang, "A Novel Wind Power Generating System Using Field Orientation Controlled Doubly-Fed Brushless Reluctance Machine," *IEEE Industry Application Society Annual Meeting Conference Record*, pp. 408-13, 1992.

[3] A. K. Wallace, R. Spée, and H. K. Lauw, "The Potential of Brushless Doubly-Fed Machines for Adjustable Speed Drives," *IEEE Industry Application Society Pulp and Paper Industry Annual Conference*, Seattle, June 20-22, 1990.

[4] C. Brune, R. Spée, and A. K. Wallace, "Experimental Evaluation of a Variable Speed, Doubly-Fed Wind Power Generation System," *IEEE Industry Application Society Annual Meeting Conference Record*, pp. 480-7, 1993.

[5] A. Kusko and C. B. Somuah, "Speed Control of a Single-Frame Cascade Induction Motor with Slip Power Pump Back," *IEEE trans. on Industry Applications*, Vol. IA-14, No. 2, pp. 97-105, April/May 1978.

[6] L. J. Hunt, "A New Type of Induction Motor," *J. of IEE*, 39, pp. 648-667, 1907.

[7] A. R. Broadway and L. Burbridge, "Self-Cascaded Machine: A Low Speed Motor or High-Frequency Brushless Alternator," *IEE Proc.*, 117(7), pp. 1277-1290, 1970.

[8] R. Li, A. K. Wallace, R. Spée, and Y. Wang, "Two Axis Model Development of Cage Rotor Brushless Doubly-Fed Machines," *IEEE Trans. on Energy Conversion*, Vol 6(3), pp.453-60, September 1991.

[9] R. Li, A. K. Wallace, and R. Spée, "Dynamic Simulation of Cage Rotor Brushless Doubly-Fed Machines," *IEEE Trans. on Energy Conversion*, Vol 6(3), pp.445-52, September 1991.

[10] R. Li, "Dynamic Modeling, Simulation, and Stability Analysis of Brushless Doubly-Fed Machines," PhD thesis, Oregon State University, May 2, 1991.

[11] R. Spée, A. K. Wallace, and H. K. Lauw, "Simulation of Brushless Doubly-Fed Drives," *IEEE Industry Application Society Annual Meeting*, San Diego, 1989.

[12] F. Creedy, "Some Development in Multi-Speed Cascade Induction Motors," *Journal of the IEE*, Vol. 39, pp. 648-667, 1907.

[13] A. E. Fitzgerald, C. Kingsley, Jr., S. D. Umans, *Electric Machinery*, 5th Ed. New York: McGraw-Hill Publishing Company, 1990.

[14] M. Liwschitz-Garik and C. C. Whipple, *Electric Machinery*, Volume I. New York: D. Van Nostrand Company, Inc., 1946.

[15] M. Liwschitz-Garik and C. C. Whipple, *Electric Machinery*, Volume II. New York: D. Van Nostrand Company, Inc., 1946.

[16] P. L Alger, *The Nature of Polyphase Induction Machines*. New York: John Wiley and Sons, Inc., 1951.

[17] P. C. Krause, *Analysis of Electric Machinery*. New York: McGraw-Hill Book Company, 1986.

[18] A. K. Wallace and A. Wright, "Novel Simulation of Cage Windings Based on Mesh Circuit Model," *IEEE PES Summer Meeting and EHV/UHV Conf.*, Vancouver, Canada, July 15-20, 1973.

[19] G. C. Alexander, R. Spee, A. K. Wallace, "Phase 3 of a Brushless Doubly-Fed Machine System Development Program," report to Bonneville Power Administration, Electric Power Research Institute, and Puget Sound Power and Light, Oregon State University 1993.

[20] A. K. Wallace, R. Spée, and A. Alajmi, "A Design for the Brushless Doubly-Fed Machine Adjustable Speed Drive," to be presented at *ICEM*, 1994.

[21] A. M. Alajmi, "Design Procedure for Brushless Doubly-Fed Machine Used as a Limited Speed-Range Pump Drive," MS thesis, Oregon State University, October 29, 1993.

[22] M. S. Boger, A. K. Wallace and R. Spée, "Investigation of Appropriate Pole Number Combinations for Brushless Doubly-Fed Machines Applied to Pump Drives," *IEEE Industry Applications Society Annual Meeting*, Denver, 1994.

[23] W. H. Beyer, Editor, *CRC Standard Mathematical Tables and Formulae*, 29th Ed. Boca Raton: CRC Press, 1991.

[24] M. S. Boger, A. K. Wallace, R. Spée, and R. Li, "General Pole Number Model of the Brushless Doubly-Fed Machine," *IEEE Industry Applications Society Annual Meeting*, Denver, 1994.

[25] B. Gorti, D. Zhou, R. Spée, G. C. Alexander, and A. K. Wallace, "Development of a Brushless Doubly-Fed Machine for a Limited Speed Pump Drive in a Waste Water Treatment Plant," *IEEE Industry Applications Society Annual Meeting*, Denver, 1994.

[26] C. V. Jones, *The Unified Theory of Electrical Machines*. London: Butterworths, 1967.

APPENDICES

Appendix A. Trigonometric Identities

The following are trigonometric relationships that are useful in resolving the transformation product.

Let:

$$n = P_p + P_c$$
$$x = -P_p \frac{2\pi}{n} = -P_p \frac{2\pi}{(P_p + P_c)}$$
$$y = -P_c \frac{2\pi}{n} = -P_c \frac{2\pi}{(P_p + P_c)}$$

Then the following relationships hold.

$$\cos(x) = \cos(y).$$

$$1 + \cos(x)\cos(y) + \cdots + \cos((n-1)x)\cos((n-1)y) = \frac{n}{2}$$
$$0 + \sin(x)\sin(y) + \cdots + \sin((n-1)x)\sin((n-1)y) = -\frac{n}{2}$$

$$1 + \cos^2(x) + \cdots + \cos^2((n-1)x) = \frac{n}{2}$$
$$1 + \cos^2(y) + \cdots + \cos^2((n-1)y) = \frac{n}{2}$$

$$\sin(x)\cos(x) + \sin(2x)\cos(2x) + \cdots + \sin((n-1)x)\cos((n-1)x) = 0$$
$$\sin(y)\cos(y) + \sin(2y)\cos(2y) + \cdots + \sin((n-1)y)\cos((n-1)y) = 0$$

$$\sin(x)\cos(y) + \sin(2x)\cos(2y) + \cdots + \sin((n-1)x)\cos((n-1)y) = 0$$
$$\cos(x)\sin(y) + \cos(2x)\sin(2y) + \cdots + \cos((n-1)x)\sin((n-1)y) = 0$$

The following summations are used in simplifying the caged-rotor impedance matrix of the first loop:

$$\sum_{k=0}^{n-1}\cos(kx)\big(\cos((k-1)x)+\cos((k+1)x)\big)=n\cos(x)=n\cos(y)$$
$$\sum_{k=0}^{n-1}\cos(ky)\big(\cos((k-1)y)+\cos((k+1)y)\big)=n\cos(x)=n\cos(y)$$

$$\sum_{k=0}^{n-1}\sin(kx)\big(\sin((k-1)x)+\sin((k+1)x)\big)=n\cos(x)=n\cos(y)$$
$$\sum_{k=0}^{n-1}\sin(ky)\big(\sin((k-1)y)+\sin((k+1)y)\big)=n\cos(x)=n\cos(y)$$

$$\sum_{k=0}^{n-1}\sin(kx)\big(\cos((k-1)x)+\cos((k+1)x)\big)=0$$
$$\sum_{k=0}^{n-1}\cos(kx)\big(\sin((k-1)x)+\sin((k+1)x)\big)=0$$

Other relationships that prove useful are directly from [17] and are shown here for reference where x and y are arbitrary angles:

$$\cos^2 x+\cos^2\left(x-\frac{2\pi}{3}\right)+\cos^2\left(x+\frac{2\pi}{3}\right)=\frac{3}{2}$$
$$\sin^2 x+\sin^2\left(x-\frac{2\pi}{3}\right)+\sin^2\left(x+\frac{2\pi}{3}\right)=\frac{3}{2}$$
$$\sin x\cos x+\sin\left(x-\frac{2\pi}{3}\right)\cos\left(x-\frac{2\pi}{3}\right)+\sin\left(x+\frac{2\pi}{3}\right)\cos\left(x+\frac{2\pi}{3}\right)=0$$
$$\cos x+\cos\left(x-\frac{2\pi}{3}\right)+\cos\left(x+\frac{2\pi}{3}\right)=0$$
$$\sin x+\sin\left(x-\frac{2\pi}{3}\right)+\sin\left(x+\frac{2\pi}{3}\right)=0$$
$$\sin x\cos y+\sin\left(x-\frac{2\pi}{3}\right)\cos\left(y-\frac{2\pi}{3}\right)+\sin\left(x+\frac{2\pi}{3}\right)\cos\left(y+\frac{2\pi}{3}\right)=\frac{3}{2}\sin(x-y)$$
$$\sin x\sin y+\sin\left(x-\frac{2\pi}{3}\right)\sin\left(y-\frac{2\pi}{3}\right)+\sin\left(x+\frac{2\pi}{3}\right)\sin\left(y+\frac{2\pi}{3}\right)=\frac{3}{2}\cos(x-y)$$

$$\cos x \sin y + \cos\left(x - \frac{2\pi}{3}\right)\sin\left(y - \frac{2\pi}{3}\right) + \cos\left(x + \frac{2\pi}{3}\right)\sin\left(y + \frac{2\pi}{3}\right) = -\frac{3}{2}\sin(x - y)$$

$$\cos x \cos y + \cos\left(x - \frac{2\pi}{3}\right)\cos\left(y - \frac{2\pi}{3}\right) + \cos\left(x + \frac{2\pi}{3}\right)\cos\left(y + \frac{2\pi}{3}\right) = \frac{3}{2}\cos(x - y)$$

$$\sin x \cos y + \sin\left(x + \frac{2\pi}{3}\right)\cos\left(y - \frac{2\pi}{3}\right) + \sin\left(x - \frac{2\pi}{3}\right)\cos\left(y + \frac{2\pi}{3}\right) = \frac{3}{2}\sin(x + y)$$

$$\sin x \sin y + \sin\left(x + \frac{2\pi}{3}\right)\sin\left(y - \frac{2\pi}{3}\right) + \sin\left(x - \frac{2\pi}{3}\right)\sin\left(y + \frac{2\pi}{3}\right) = -\frac{3}{2}\cos(x + y)$$

$$\cos x \sin y + \cos\left(x + \frac{2\pi}{3}\right)\sin\left(y - \frac{2\pi}{3}\right) + \cos\left(x - \frac{2\pi}{3}\right)\sin\left(y + \frac{2\pi}{3}\right) = \frac{3}{2}\sin(x + y)$$

$$\cos x \cos y + \cos\left(x + \frac{2\pi}{3}\right)\cos\left(y - \frac{2\pi}{3}\right) + \cos\left(x - \frac{2\pi}{3}\right)\cos\left(y + \frac{2\pi}{3}\right) = \frac{3}{2}\cos(x + y)$$

Appendix B. Technical Papers

General Pole Number Model of the Brushless Doubly-Fed Machine

Michael S. Boger, Student Member, IEEE
Alan Wallace, Senior Member, IEEE
René Spée, Senior Member, IEEE
Department of Electrical and Computer Engineering
Oregon State University
Corvallis, Oregon 97331 U.S.A.

Ruqi Li, Member, IEEE
Electrical Division
Failure Analysis Associates, Inc.
149 Commonwealth Dr.
Menlo Park, CA 94025 U.S.A.

***Abstract*—The brushless doubly-fed machine is receiving attention as a contender for several niche applications. In some cases the speed ranges of these applications appear to be more readily met by judicious selection of the pole-pair numbers of the stator phase windings. In order to compare different proposed pole-pair configurations and to help in the development of specific designs, a general analytical model, in both dynamic and steady state forms, is presented. This model supersedes previous analyses which are restricted to the 3/1 pole-pair combination of early laboratory machines. The new model is also completely valid for both positive and negative control voltage sequences. The increased modelling flexibility enables sound estimations of the drive converter ratings, the reduction of which is the key to the economic advantage of these machines. An example of the correlation of the performance predictions and test results encourages use of this new model.**

I. Introduction

Recently, there have been noticeable interest and research activities in using brushless doubly-fed reluctance machines [1,2] and brushless doubly-fed induction machines [3,4] for adjustable speed drives (ASD) and variable speed generators (VSG). The brushless doubly-fed induction machine (BDFM) shows great promise in reducing the rating of the power electronic converter needed for ASD and VSG applications to a small fraction of the machine rating. Early work dealt with two separate wound rotor induction machines cascaded together [5] to provide speed control. The BDFM [6,7] eliminates the need for a wound rotor induction machine, and when used with a bi-directional power electronic converter, has the ability to provide precise speed control by virtue of its two stator windings and modified cage rotor. The BDFM shows promising results in automotive, wind generation, and pump drive applications, as well as other variable speed niche applications [3]. Figure 1 shows a typical BDFM schematic in comparison with that of an equivalent induction motor drive.

Stator pole-pair combinations investigated to date include 2/1, 3/1, and 6/2, with 2, 3 and 6 power winding pole-pairs and 1 and 2 control winding pole-pairs, respectively. Two axis model development, however, has addressed the 3-1 geometry exclusively [8,9]. Thus, there is a need to develop a model which is appropriate for any combination of pole-pair numbers. The expanded choice of pole combinations allows for flexible designs enabling tailoring of the drive to custom speed ranges and torque requirements. The analysis of the 3-1 machine results in a very simplified model because there are only four rotor nests (see Fig. 2) which, when analyzed in a two axis reference frame, results in immediate orthogonalities.

The present paper extends the modeling technique to any number of poles, enabling accurate design of new proposed BDFMs. The model shows the inclusion of terms in the mutual inductance parameters which did not appear in the 3-1 model because of cancellation due to the orthogonal axes of the 3-1 machine's rotor. Without this model, there can only be rough calculations based on classical induction motor equations which do not adequately define the relationship

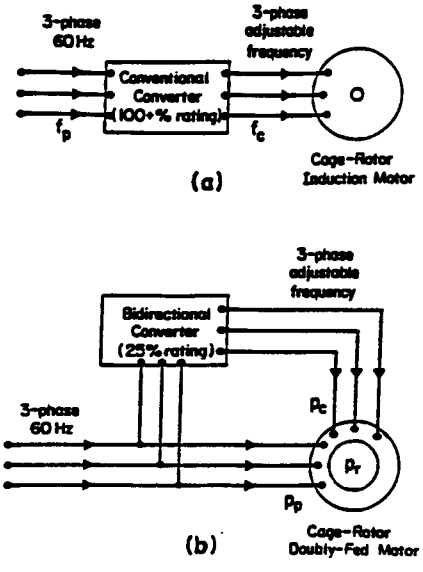

Fig. 1. Induction machine and BDFM drive configurations.

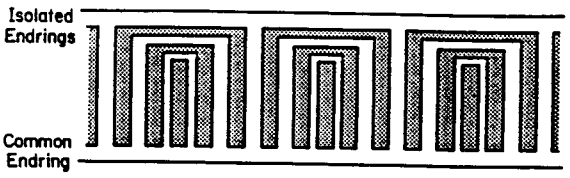

Fig. 2. Rotor configuration of the BDFM

between two stator windings sharing a common rotor. In addition, this model can be easily extended to handle cageless BDFM rotors. This general pole model, in two axes, will result in a reduced simulation time due to a reduction of the number of state equations needing to be solved in comparison to a detailed simulation [10]. A power invariant direct-quadrature axes (dq) transformation is applied in the rotor reference frame to the voltage equations to arrive at the simplified model. A companion paper [11] shows the results of simulations comparing the performance of a 3/1 machine with a different pole pair numbered machine.

II. Structure and Model Development of the BDFM

Consider a BDFM with P_p pole-pairs in the power winding and P_c pole-pairs in the control winding. The windings are assumed sinusoidally distributed and $P_p \neq P_c$ to avoid direct transformer coupling. The rotor consists of $n = (P_p + P_c)$ nests each with m loops in a configuration due to Broadway [7] as illustrated in Fig. 2. This nested isolated loop structure allows the indirect coupling of the two stator windings to take place efficiently by constraining the induced rotor currents.

A. System Equations in Machine Variables

The following derivation assumes balanced 3 phase windings and considers only the fundamental component of the stator phase to rotor loop mutuals. Cross coupling of the stator phases occurs only through the rotor. The general voltage equation can be expressed as follows, with nomenclature given at the end of the paper.

$$\begin{bmatrix} v_{sp} \\ v_{sc} \\ v_r \end{bmatrix} = \begin{bmatrix} Z_{sp} & 0 & Z_{spr} \\ 0 & Z_{sc} & Z_{scr} \\ Z'_{spr} & Z'_{scr} & Z_r \end{bmatrix} \begin{bmatrix} i_{sp} \\ i_{sc} \\ i_r \end{bmatrix} \tag{1}$$

The stator impedance matrices are similar to regular induction motor matrices as derived in [8]. The power winding stator impedance matrix is shown in (2); the control winding matrix is similar. The rotor impedance matrix is partitioned into sub-matrices that show the impedances of all similar loops in a nest as shown in (3). Since there are m loops per nest, the rotor partitioned impedance matrix is square of dimension m. Each partitioned matrix is square of dimension n. Loops are numbered starting from the outside of a nest and working inward. The rotor cage of n bars, if present, would be loop #1 in each of the nests. The combination of this rotor impedance matrix with the stator impedance matrix forms an electrical system of order $6+mn$.

$$Z_{sp} = \begin{bmatrix} r_p + (L_{lp} + L_{mp})D_t & -\frac{1}{2}L_{mp}D_t & -\frac{1}{2}L_{mp}D_t \\ -\frac{1}{2}L_{mp}D_t & r_p + (L_{lp} + L_{mp})D_t & -\frac{1}{2}L_{mp}D_t \\ -\frac{1}{2}L_{mp}D_t & -\frac{1}{2}L_{mp}D_t & r_p + (L_{lp} + L_{mp})D_t \end{bmatrix} \tag{2}$$

$$Z_r = \begin{bmatrix} Z_{11} & Z_{12} & \cdots & Z_{1m} \\ Z_{21} & Z_{22} & \cdots & Z_{2m} \\ \vdots & \vdots & \ddots & \vdots \\ Z_{m1} & Z_{m2} & \cdots & Z_{mm} \end{bmatrix} \tag{3}$$

A typical partitioned rotor impedance matrix is shown in (4). The primed quantities arise from the presence of the common bar impedance of the caged rotor. The resistance term is the resistance of the bar and the inductance term is the slot leakage associated with the common bar. The common bar terms vanish if a cage-less rotor is used. For other rotor impedance matrices, replace the *11* subscript with the particular impedance to be evaluated, *ij*.

$$Z_{11} = \begin{bmatrix} r_{11} + L_{11}D_t & -r'_{12} - (L'_{11} + M_{11})D_t & \cdots & -r'_{1n} - (L'_{11} + M_{11})D_t \\ -r'_{11}(L'_{12} + M_{11})D_t & r_{11} + L_{11}D_t & \cdots & -M_{11}D_t \\ \vdots & \vdots & \ddots & \vdots \\ -r'_{11} - (L'_{11} + M_{11})D_t & -M_{11}D_t & \cdots & r_{11} + L_{11}D_t \end{bmatrix} \tag{4}$$

The mutual inductance between the power winding and rotor can be partitioned into a row of matrices which represent the mutual of the stator winding with all of the similar loops of all nests. The mutual impedance matrix between the power winding and the rotor, (5), uses the pole pairs of the

winding and the mechanical angle to resolve the necessary impedances.

$$Z_{spr} = D_i L_{spr} = D_i[L_{spr1}\ \ L_{spr2}\ \cdots\ L_{sprm}] \qquad (5)$$

A typical term in the mutual inductance matrices is shown as (6) in which the pole-pair number, P, will be either P_p or P_c depending on which winding is under consideration. A nominal angle, α, can exist between the power winding A-phase reference axis and the control winding A-phase axis which accounts for the physical displacement of the phases along the circumference of the motor. The row dictates the value of k to use depending on which phase is being coupled. The value of j dictates coupling to a specific rotor loop and is the column index.

$$M_{sri}\cos\left(P\left(\theta_r - \beta - \frac{k2\pi}{3P} + \frac{j2\pi}{n}\right)\right) \qquad (6)$$

$$k\in[0,\ 1,\ 2],\ j\in[0,\ 1,\ \cdots,\ (n-1)],\ \beta = \{0,\ \alpha\}$$

B. DQ Transformation

The dq reference frame power invariant transformation matrices are developed for transformation to the rotor mechanical reference frame. Transformation to any other reference frame will not eliminate the time varying mutual inductances. The mechanical rotor angle is used to account for the different wave numbers impressed on the rotor due to the different poles of the windings. This transformation simplifies the equations of the electrical system, resulting in 6 electrical equations. The rotor is assumed initially aligned with the power winding axis for ease of computation without loss of generality. Reference [12] presents a method of developing a general phase transformation matrix which is adaptable to both power and control winding transformations. A typical term of these matrices is shown, (7), neglecting the zero sequence terms due to analysis of balanced winding voltages which results in a rectangular matrix of dimension 2 by 3. In (7), the value of k dictates a column quantity. The second row of the transformation is composed of sine functions.

$$\sqrt{\frac{2}{3}}\cos\left(P\left(\theta_r - \beta - \frac{k2\pi}{3P}\right)\right) \qquad (7)$$

$$k\in[0,\ 1,\ 2],\ \beta = \{0,\ \alpha\}$$

Using the principle of superposition, the rotor voltages and currents are broken into components, (8) and (9), which are the result of influence from the power and control windings separately. This introduces two more states in the rotor which will subsequently be combined to yield the desired model.

$$v_{pr} = \begin{bmatrix} v_{qpr} \\ v_{dpr} \end{bmatrix},\quad v_{cr} = \begin{bmatrix} v_{qcr} \\ v_{dcr} \end{bmatrix} \qquad (8)$$

$$i_{pr} = \begin{bmatrix} i_{qpr} \\ i_{dpr} \end{bmatrix},\quad i_{cr} = \begin{bmatrix} i_{qcr} \\ i_{dcr} \end{bmatrix} \qquad (9)$$

Each rotor loop must be taken into account in the transformation. However, because of the alignment of the loops within the nests, the transformation can be simplified. Thus, each rotor loop is transformed into a set of d-axis and q-axis coils. All of the d-axis coils can be summed on the rotor by construction of the rotor transformation matrix as a partitioned row matrix, (10), to yield an equivalent single d-axis rotor coil to minimize the computation requirements; similarly for the q-axis coils. A typical term of the rotor loop transformation matrices is shown as (11). First row terms are cosine functions; second row terms are sine functions. Each rotor transformation matrix uses the appropriate number of pole pairs.

$$C_{rp} = [C_{rp1}\ \ C_{rp2}\ \cdots\ C_{rpm}] \qquad (10)$$

$$C_{rpj} = \sqrt{\frac{2}{mn}}\cos\left(-P\frac{j2\pi}{n}\right) \qquad (11)$$

$$j\in[0,\ 1,\ \cdots,\ (n-1)]$$

The matrix transformation multiplication to be performed is shown in (12). The transformation of the stator windings is straightforward. However, transformation of the stator to rotor mutual inductances presents a difficulty because of the form of the stator and rotor transformation matrices. A closed form solution is found due to symmetry based on the sum of the pole-pairs of the two windings as reflected in the values of the parameters used in the model.

$$[Z_{qd}] = \begin{bmatrix} C_{sp} & 0 & 0 & 0 \\ 0 & C_{sc} & 0 & 0 \\ 0 & 0 & C_{rp} & 0 \\ 0 & 0 & 0 & C_{rc} \end{bmatrix} \begin{bmatrix} Z_{sp} & 0 & Z_{spr} & Z_{spr} \\ 0 & Z_{sc} & Z_{scr} & Z_{scr} \\ Z_{spr}^T & 0 & Z_r & 0 \\ 0 & Z_{scr}^T & 0 & Z_r \end{bmatrix} \begin{bmatrix} C_{sp}^T & 0 & 0 & 0 \\ 0 & C_{sc}^T & 0 & 0 \\ 0 & 0 & C_{rp}^T & 0 \\ 0 & 0 & 0 & Z_{rc}^T \end{bmatrix} \qquad (12)$$

The rotor voltages and currents need to be combined to eliminate the excess states introduced earlier. Equation (13) shows how an arbitrary abc reference frame variable on the

$$r_r = \frac{1}{m}\left(\sum_{j=1}^{m}\sum_{i=1}^{m} r_{ij} - 2\cos\left(-P_p\frac{2\pi}{n}\right)r'_{11}\right)$$

$$L_r = \left(\frac{1}{m}\right)\left(\sum_{i=1}^{m}(L_{ii} + M_{ii}) + \sum_{j=1}^{m}\sum_{i=1,i\neq j}^{m}(M_{ij} + M'_{ij}) - 2\cos\left(-P_p\frac{2\pi}{n}\right)L'_{11}\right) \quad (21)$$

E. Steady State Model

The steady state analysis assumes that the machine is synchronized so that the frequencies of the windings in the two axes are constrained by (22) allowing either positive or negative sequence control voltage. Maintaining this constraint enables power to be transferred from one winding to the other through the rotor.

$$(\omega_p - P_p\omega_r) = (P_c\omega_r \mp \omega_c) \quad (22)$$

The steady state voltages, after transformation, can be substituted into the dynamic model to result in three voltage equations that describe the steady state performance of the BDFM, (23)-(25). The first sign on the control voltage signifies positive sequence control voltage, the second sign negative sequence voltage. The rotor current frequency is given by either side of (22), the left side chosen for ease of analysis. The torque equation, expressed in the real and imaginary parts of the rms currents, is given by (26).

$$V_{qp} = (r_p + j\omega_p L_p)I_{qp} + j\omega_p M_p I_{qr} \quad (23)$$

$$V_{qc} = (r_c \mp j\omega_c L_c)I_{qc} \mp j\omega_c M_c I_{qr} \quad (24)$$

$$V_{qr} = r_r I_{qr} + j(\omega_p - P_p\omega_r)(L_r I_{qr} + M_p I_{qp} + M_c I_{qc}) \quad (25)$$

$$T_e = 2P_p M_p(Im(I_{qp})Re(I_{qr}) - Re(I_{qp})Im(I_{qr})) - 2P_c M_c(Im(I_{qc})Re(I_{qr}) - Re(I_{qc})Im(I_{qr})) \quad (26)$$

The steady state equivalent model can be represented by three circuits in the rotor reference frame where the voltages and currents are at the rotor current frequency and effects from the windings are represented by current controlled voltage sources as shown in Fig. 3.

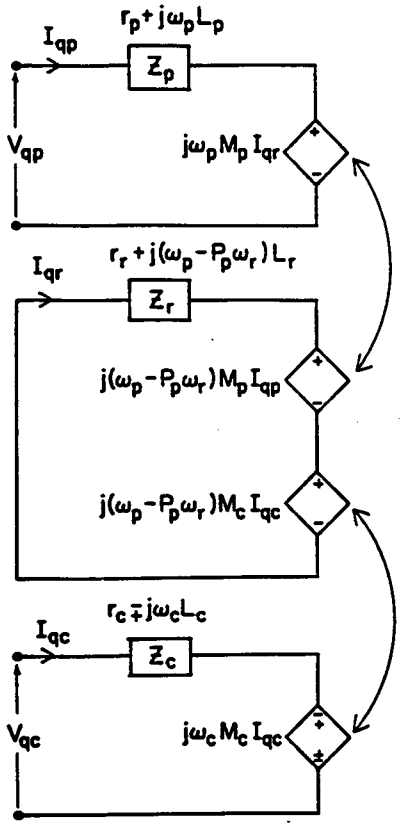

Fig. 3. BDFM steady state model in the rotor reference frame.

F. Simulation Results

Steady state performance predictions can be made using the steady state model in this paper. In order to examine the applicability of the model, simulations of the steady state performance of a 5 hp, 3/1 pole-pair, laboratory machine were prepared for comparison with available test results. These comparisons are shown in Figs. 4-6. The parameters of the machine required for the simulation are given in the appendix. The load being driven in this example is a representation of a simple fan or centrifugal pump characteristic in which the torque is a function of the square of the shaft speed. For this machine, the two extreme load torques are 13.75 N-m at 587 r/min and 31.5 N-m at 867 r/min.

The correlation between predictions and the test results for the stator winding currents and the power winding power factors, shown in Figs. 4 and 5, respectively, demonstrates the use of this model as a post-design assessment tool. The predictions of the motor efficiency, Fig. 6, show a substantial but consistent optimism compared to the test data. It should be noted that the measured values are line-input to shaft-

rotor can be combined from the earlier separation. The system of equations in (13) is an over determined system with only two independent equations. Extracting two acceptable solutions yields (14) as the describing equations for the rotor quantities.

$$[f_r] = [C_{rp}^T][v_{pr}] + [C_{rc}^T][v_{cr}] \tag{13}$$

$$\begin{aligned} v_{qr} &= v_{qpr} + v_{qcr} \\ v_{dr} &= v_{dpr} - v_{dcr} \\ i_{qr} &= i_{qpr} + i_{qcr} \\ i_{dr} &= i_{dpr} - i_{dcr} \end{aligned} \tag{14}$$

C. Torque Equation

The torque equation has been determined assuming a linear magnetic system. The basis for developing the torque equation, the abc reference frame equation (15), is shown below. The square partitioned impedance matrix allows the summation of all torques developed due to the coupling from one winding, through the rotor, to the other winding.

$$T_e = [i_s]^T \frac{\partial}{\theta_r} \begin{bmatrix} Z_{spr} & Z_{spr} \\ Z_{scr} & Z_{scr} \end{bmatrix} [i_r] \tag{15}$$

Utilizing the transformation matrices, the dq reference frame torque equation is found by the product shown in (16). The additional rotor current constraints, (14) are used to simplify the equation resulting in the final simplified form shown in (17).

$$T_e = [i_{qds}]^T \begin{bmatrix} C_{sp} & 0 \\ 0 & C_{sc} \end{bmatrix} \frac{\partial}{\theta_r} \begin{bmatrix} Z_{spr} & Z_{spr} \\ Z_{scr} & Z_{scr} \end{bmatrix} \begin{bmatrix} C_{rp}^T & 0 \\ 0 & C_{rc}^T \end{bmatrix} [i_{qdr}] \tag{16}$$

$$T_e = M_p P_p (i_{qp} i_{dr} - i_{dp} i_{qr}) - M_c P_c (i_{qc} i_{dr} + i_{dc} i_{qr}) \tag{17}$$

D. Dynamic Model

Obviously there is no rotor applied voltage, so that combining the rotor simplifying equations, (14), along with the results of the transformation product, (12), a dynamic machine voltage model results, (18).

The stator inductances, (19), are as expected from standard dq analysis of an induction machine.

$$\begin{aligned} L_p &= \left(L_{lp} + \frac{3}{2} L_{mp} \right) \\ L_c &= \left(L_{lc} + \frac{3}{2} L_{mp} \right) \end{aligned} \tag{19}$$

The other variables within (18) are found through simplifying the series of *n* terms that results from the transformation product (12). This leads to a sum of multiplications between sinusoids which can be simplified based on the symmetry of the problem. After simplifying, the mutual inductances in the equivalent model are as shown in (20).

$$\begin{aligned} M_p &= \left(\frac{n}{2} \right) \sqrt{\frac{3}{mn}} \sum_{j=1}^{m} M_{sprj} \\ M_c &= \left(\frac{n}{2} \right) \sqrt{\frac{3}{mn}} \sum_{j=1}^{m} M_{scrj} \end{aligned} \tag{20}$$

The evaluation of the rotor resistance and inductance is as shown in (21). It is significant to note that the cosine terms in (21) reduce to zero with the 3/1 pole-pair architecture analyzed previously [8]. The value of the cosine terms can assume either positive or negative values depending on the pole pair combinations which shows the sensitivity of the BDFM to rotor leakage inductance.

$$\begin{bmatrix} v_{qp} \\ v_{dp} \\ v_{qc} \\ v_{dc} \\ 0 \\ 0 \end{bmatrix} = \begin{bmatrix} r_p + L_p D_t & P_p \omega_r L_p & 0 & 0 & M_p D_t & P_p \omega_r M_p \\ -P_p \omega_r L_p & r_p + L_p D_t & 0 & 0 & -P_p \omega_r M_p & M_p D_t \\ 0 & 0 & r_c + L_c D_t & P_c \omega_r L_c & M_c D_t & -P_c \omega_r M_c \\ 0 & 0 & -P_c \omega_r L_c & r_c + L_c D_t & -P_c \omega_r M_c & -M_c D_t \\ M_p D_t & 0 & M_c D_t & 0 & r_r + L_r D_t & 0 \\ 0 & M_p D_t & 0 & -M_c D_t & 0 & r_r + L_r D_t \end{bmatrix} \begin{bmatrix} i_{qp} \\ i_{dp} \\ i_{qc} \\ i_{dc} \\ i_{qr} \\ i_{dr} \end{bmatrix} \tag{18}$$

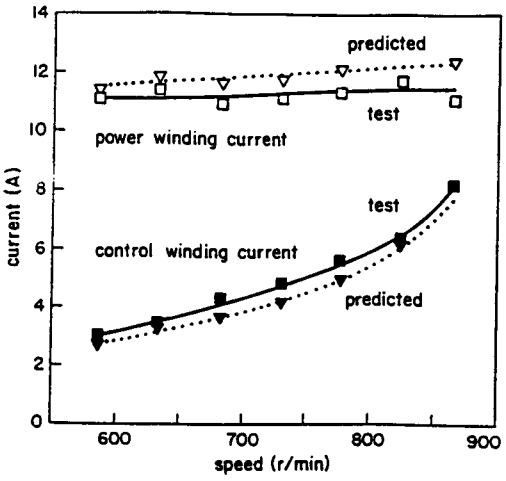

Fig. 4. Comparison of predicted and measured stator currents.

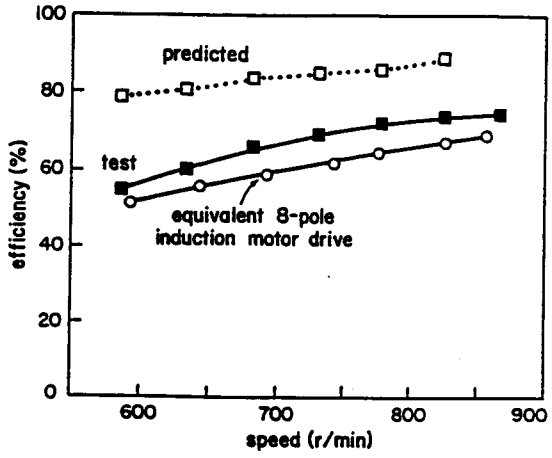

Fig. 6. Comparison of predicted and measured motor efficiencies.

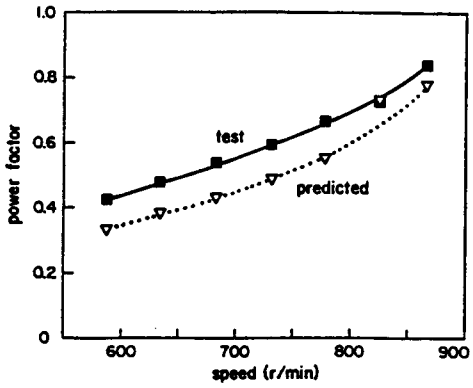

Fig. 5. Comparison of predicted and measured power factor of the power winding.

output quantities which will contain converter loss, machine core loss, machine stray load loss, and bearing friction and windage loss. None of these losses are currently included in the model. Methods are available for estimating converter, bearing, and windage losses. However, in a machine of such complex electromagnetic interactions as the BDFM, identification of core and stray load losses represents a substantial challenge. Also shown in Fig. 6 for comparison is the measured efficiency of a commercially produced 8-pole inductor motor VSG.

III. Conclusions

By a combination of involved transformation techniques and circuit theorems, the original electrical system of the BDFM, which is of order $6+mn$, has been reduced to a minimum possible equivalent system of order 6. The reduced system of equations results in substantially decreased simulation times.

The model yields highly acceptable correlation of the laboratory test phase currents and power factor for the 3/1 pole-pair machine. Future work will investigate the correlation for the other pole-pair configurations. Additional analysis is required to develop techniques to account for core and stray load losses in the machine.

Analysis of the general pole number model showed how the values of the rotor parameters can be affected by the common bar impedance. As a consequence, if a certain pole pair combination is to be used, evaluating the effect of the common bar impedance may dictate the use of a cage-less rotor instead of the standard caged rotor for future BDFM designs.

IV. Nomenclature

A. Main Variables

- C transformation matrix.
- Dt differentiation with respect to time.
- i instantaneous current.
- I rms current.
- j imaginary operator.

L inductance.
L' common bar inductance.
m number of rotor loops.
M mutual inductance.
n number of rotor nests = P_p+P_p.
P number of pole-pairs.
r resistance.
r' common bar resistance.
Te electrical torque.
v instantaneous voltage.
V rms voltage.
ω angular frequency.
ω_r speed of the rotor.
Z impedance matrix.
Z' transformed impedance matrix with excess states.

B. Subscript and Superscript Variables

c control winding.
d d-axis quantity.
i rotor loop index.
j rotor loop index.
l leakage quantity.
p power winding.
q q-axis quantity.
r rotor quantity.
s stator quantity.
T transpose of a matrix.

APPENDIX

The following parameters are derived from a 5 hp BDFM currently being used as a laboratory prototype.

r_p = 0.672 Ω, r_c = 0.924 Ω
L_p = 66.5 mH, L_c = 378.4 mH
r_r = 164 μΩ, L_r = 42.9 μH
M_p = 839 μH, M_c = 3.195 mH
α = 70.1 deg.

ACKNOWLEDGEMENTS

The authors wish to thank the Electric Power Research Institute, Bonneville Power Administration, and Puget Sound Power and Light for their financial support for this project.

REFERENCES

[1] Y. Liao and C. Sun, "A Low Cost, Robust Sensorless Controlled Scheme for Doubly-Fed Reluctance Motor Drives," *IEEE Industry Application Society Annual Meeting Conference Record*, pp. 437-44, 1993.

[2] Y. Xu and Y. Tang, "A Novel Wind Power Generating System Using Field Orientation Controlled Doubly-Fed Brushless Reluctance Machine," *IEEE Industry Application Society Annual Meeting Conference Record*, pp. 408-13, 1992.

[3] A.K. Wallace, R. Spée, and H.K. Lauw, "The Potential of Brushless Doubly-Fed Machines for Adjustable Speed Drives," *IEEE Industry Application Society Pulp and Paper Industry Annual Conference*, Seattle, June 20-22, 1990.

[4] C. Brune, R. Spée, and A. K. Wallace, "Experimental Evaluation of a Variable Speed, Doubly-Fed Wind Power Generation System," *IEEE Industry Application Society Annual Meeting Conference Record*, pp. 480-7, 1993.

[5] A. Kusko and C. B. Somuah, "Speed Control of a Single-Frame Cascade Induction Motor with Slip Power Pump Back," *IEEE Trans. on Industry Applications*, Vol. IA-14, No. 2, pp. 97-105, April/May 1978.

[6] L.J. Hunt, "A New Type of Induction Motor," *J. of IEE*, 39, pp. 648-667, 1907.

[7] A.R. Broadway and L. Burbridge, "Self-Cascaded Machine: A Low Speed Motor or High-Frequency Brushless Alternator," *IEE Proc.*, 117(7), pp. 1277-1290, 1970.

[8] R. Li, A.K. Wallace, R. Spée, and Yixin Wang, "Two Axis Model Development of Cage Rotor Brushless Doubly-Fed Machines," *IEEE Trans. on Energy Conversion*, Vol 6(3), pp.453-60, September 1991.

[9] R. Li, A.K. Wallace, and R. Spée, "Dynamic Simulation of Cage Rotor Brushless Doubly-Fed Machines," *IEEE Trans. on Energy Conversion*, Vol 6(3), pp. 445-52, September 1991.

[10] R. Spée, A.K. Wallace, and H.K. Lauw, "Simulation of Brushless Doubly-Fed Drives," *IEEE Industry Application Society Annual Meeting*, San Diego, 1989.

[11] A.K. Wallace, R. Spée, and M.S. Boger, "Investigation of Appropriate Pole Number Combinations for Brushless Doubly-Fed Machines Applied to Pump Drives," *IEEE Industry Applications Society Annual Meeting*, Denver, 1994.

[12] A.K. Wallace and A. Wright, "Novel Simulation of Cage Windings Based on Mesh Circuit Model," *IEEE PES Summer Meeting and EHV/UHV Conf.*, Vancouver, Canada, July 15-20, 1973.

Investigation of Appropriate Pole Number Combinations for Brushless Doubly-Fed Machines Applied to Pump Drives

Michael S. Boger, Student Member, IEEE
Alan Wallace, Senior Member, IEEE
René Spée, Senior Member, IEEE
Department of Electrical and Computer Engineering
Oregon State University
Corvallis, Oregon 97331 U.S.A.

Abstract—**Brushless doubly-fed machines have the capability of precise (synchronous) speed control over a wide speed range through the use of a bi-directional power converter due to the magnetic coupling of two different pole numbered stator windings through a specifically configured rotor. The application of brushless doubly-fed machines with different pole-pair combinations is investigated for use as a limited speed range pump drive by using a steady state equivalent model developed in a companion paper. The proposed brushless doubly-fed machine designs when compared to an equivalent induction motor drive show the advantages of operation at close to unity power factor and reduced power converter rating. These results from the simulation demonstrate the substantial economic advantage of using the brushless doubly-fed machine in limited speed-range operations.**

I. Introduction

Recent investigations of doubly-fed machines have illustrated their capability for wide ranges of precise speed control by the application of a single bi-directional power converter of controlled voltage and frequency [1,2]. Potential application areas include adjustable speed drives (ASDs) and variable speed generators (VSGs) [3-5]. Compared to singly-fed machines, doubly-fed devices have the advantage of reduced rating of the power electronic converter because only one winding needs to be controlled to provide speed adjustment. For limited speed ranges such as a 2:1 ratio, typical in many industrial applications, the converter rating can be reduced to as low as 25% of the rating of the machine. Consequently, the cost of the power electronic converter can be decreased significantly; this saving is especially notable when dealing with medium to high power drives or critical drives where redundant converters are employed. A further advantage is derived from the fact that the bulk of the power enters or leaves the machine directly unprocessed by power electronics. Thus, power quality standards, such as IEEE 519 and IEC 555, are much more readily met or exceeded.

A particular type of doubly-fed machine is the self-cascaded induction machine, or brushless doubly-fed machine (BDFM). It has two stator windings of different pole-pair numbers which interact through a rotor having a modified cage form referred to as nests [6,7] as depicted schematically in Fig. 1. The two stator windings are referred to as the power winding and the control winding, the latter being supplied via the power electric converter as shown in Fig. 2. The 3/1 machine, where 3 refers to the power winding pole pairs and 1 to the control winding pole pair, has been

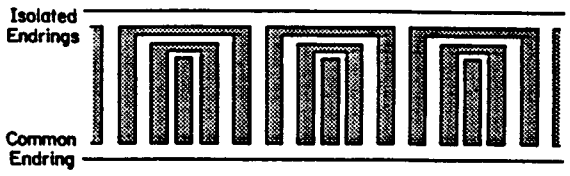

Fig. 1. BDFM rotor configuration.

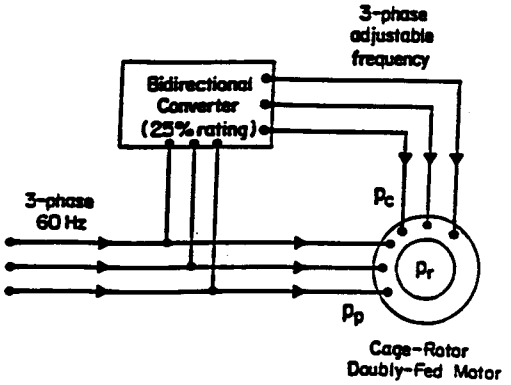

Fig. 2. BDFM system configuration.

analyzed earlier [8-10]. The 3/1 combination shows great promise for a wind-power generator in the speed range of 1000 to 1800 r/min [4] and as a pump drive for the range 600-900 r/min. One such drive has been constructed and is soon to be installed in a municipal waste water treatment plant to serve as a field demonstration unit of this technology [11]. Although other BDFM pole-pair combinations are possible, research and demonstration activities to date have concentrated on the 3/1 configuration. Consequently, investigations of application specific selection of pole-pair numbers was not possible prior to the development of the analysis presented in the companion paper [12].

The recently developed general analysis is to be used here to illustrate the tradeoffs associated with a particular application design. Analysis and performance prediction for a low power laboratory BDFM driving a nonlinear torque speed characteristic load are given in [12]. The resulting confidence in the model and experience in its application justify the trade-off study for a 45 kW demonstration pump drive. The steady state circuit model is used to analyze alternative design configurations of the BDFM with regard to pole number selection for performance optimization and converter minimization. This paper will serve to illustrate the design capabilities of the general pole number model by comparing the results with the previous 3/1 model [8-10], while extending the modeling to new pole number designs.

II. The Application Project

The BDFM is currently being considered for several applications and is actively being developed for a pump drive for a waste water treatment facility. The design targets of this 45 kW drive [11], given in Table I, are comparable to those of the alternative 6-pole induction motor drive, shown schematically in Fig. 3, which might otherwise be selected for this duty. The unit is to replace an existing slip-ring induction motor (SRIM) with rheostatic rotor speed control, which has been characterized as having a performance substantially inferior to the design targets in all but the torque capability. Consequently, if the design targets can be met by a BDFM drive, the pump will be more flexibly controlled and more economically operated at lower capital cost than by any alternative system. A 3/1 BDFM system, currently under construction, was selected based on laboratory experience of the configuration, but alternative machines could be equally applicable. It is the objective of this study to investigate the most viable BDFM configuration for this application based on the following criteria:

(i) overall system cost based on converter rating and machine complexity;

(ii) ability of the system to meet the targets of Table I, particularly the torque characteristic of the pump which approximates a function proportional to the square of speed.

TABLE I
Design Targets

Quantity	Target
Speed Range	600-900 rpm
Torque Range	250-450 Nm
Power Factor	0.84 @ rated output
Efficiency	90% @ rated output

By way of a baseline for comparison, the speed of the induction motor drive is given by:

$$N = 60 \times \frac{f_c}{P_I}(1-s) \qquad r/\text{min} \qquad (1)$$

in which s is the slip required to meet the load torque, f_c is the frequency of the converter, and P_I is the number of pole-pairs of the induction motor. Also, the rating of the power converter required for the induction motor is given by:

$$S_{cI} = \frac{P_{max}}{\eta(p.f.)} \qquad (2)$$

where P_{max} is the peak shaft power required for the pump, η is its efficiency, and $(p.f.)$ is its power factor at this condition.

Based on the speed requirements and horsepower rating of the machine, a precise range of BDFM converter frequency can be developed which can be used as a guide to values for the converter rating. The BDFM is a synchronous device for which the converter frequency range is determined from the following, where N is the motor speed in rpm, f_p and f_c are the power and converter winding frequencies, respectively, and P_p and P_c are the pole pair numbers of the power and control windings, respectively:

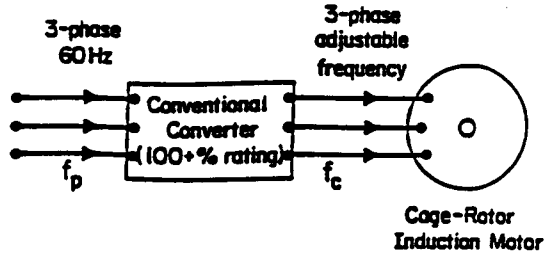

Fig. 3. Induction motor drive configuration.

$$N = 60\,\frac{f_p \pm f_c}{P_p + P_c} \quad r/min\ . \tag{3}$$

The rating of the converter can be estimated from the following, where S_{cB} is the kVA rating of the converter, S_m is the motor rating, f_c is the peak converter frequency, and f_p is the supply frequency (60 Hz):

$$S_{cB} \approx S_m\,\frac{\hat{f}_c}{\hat{f}_c + f_p}\ . \tag{4}$$

From the above expressions it is evident that the converter rating for the induction motor drive is dictated primarily by the upper speed limit, whereas the corresponding rating for BDFM converters is also a function of the number of poles. This is summarized in Table II where a negative frequency signifies a voltage sequence opposite to the power winding sequence.

III. Steady-State Model

The operation of a waste water pump does not call for high performance dynamic control [13]. Consequently, it is adequate to examine the performance of the BDFM options using a steady-state model derived from the analysis presented in the companion paper. In steady-state, the two axes of the d-q model are effectively equivalent and give rise to the equivalent circuit of Fig. 4 and the motoring condition equations [12]

$$V_{qp} = \left[r_p + jw_pL_p + \frac{w_p(w_p - P_pw_r)M_p^2}{(r_r + j(w_p - P_pw_r)L_r)} \right] I_{qp} + \frac{w_p(w_p - P_pw_r)M_pM_c}{(r_r + j(w_p - P_pw_r)L_r)}\, I_{qc} \tag{5}$$

and

$$V_{qc} = \left[r_c \mp jw_cL_c \mp \frac{w_c(w_p - P_pw_r)M_c^2}{(r_r + j(w_p - P_pw_r)L_r)} \right] I_{qc} \mp \frac{w_c(w_p - P_pw_r)M_pM_c}{(r_r + j(w_p - P_pw_r)L_r)}\, I_{qp}\ .$$

The process of cross coupling, from power winding to control winding via the rotor and vice-versa is obviously most dependent on the product of the mutual inductances which the stator windings have with the rotor loops: i.e., a key factor in the design of an effective BDFM rotor is the cross coupling factor

$$k_{pc} = M_pM_c\ . \tag{6}$$

In the derivation of expressions for these mutual inductances in terms of machine geometry for individual loops, the coil-span factors of the rotor loops expressed in terms of the stator pole-pair numbers feature prominently. Hence,

$$k_{pc} \propto \sin\left[P_p\frac{\theta_R}{2}\right] \sin\left[P_c\frac{\theta_R}{2}\right]\ . \tag{7}$$

This function for the three candidate configurations is shown in Fig. 5 where the rotor loop span angle, θ_R, is expressed as a fraction of its maximum possible value, θ_{Rmax}, (i.e., the outermost loop span), where

$$\theta_{Rmax} = \frac{360^\circ}{P_p + P_c}\ . \tag{8}$$

It is shown in Fig. 5 that the potential for producing good coupling between the two winding systems is far better for

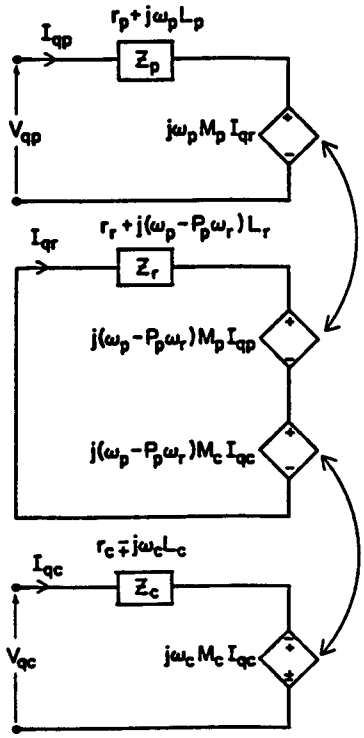

Fig. 4. BDFM steady state equivalent circuit.

TABLE II
ESTIMATED POWER ELECTRONIC CONVERTER REQUIREMENTS

Machine	3/1 Pole-Pair BDFM	4/1 Pole-Pair BDFM	4/2 Pole-Pair BDFM	3 Pole-Pair Induction Machine
Converter Frequency Range, Hz	$-20 \le f_c \le 0$	$-10 \le f_c \le 15$	$0 \le f_c \le 30$	$35 \le f_c \le 50$
Converter Rating, kVA	15	12	20	60

the 4/2 pole-pair configuration than the other two options. Thus, from a consideration of overall system design features, the 4/2 pole-pair BDFM was chosen for design comparison with the 3/1 pole-pair demonstration machine. However, it should be noted at this stage that stable BDFM operating torques are based on rotor currents produced by inductive mechanisms. Hence, the BDFM produces no useful torque at speeds given by

$$N = 60 \times \frac{f_p}{P_p} \qquad (9)$$

i.e., at 1200 r/min for the 3/1 machine and at 900 r/min for both the 4/1 and 4/2 machines. Hence, of the alternative designs only the 3/1 configuration will operate at the required top speed. Also, the results of the performance prediction are needed to determine, with any confidence, how close to the required 900 r/min stable synchronous operation can be maintained to meet the required load torque.

IV. ALTERNATIVE MACHINE DESIGNS

Details of the two BDFM designs for comparison purposes are given in Table III. Certain parameters cannot be divulged here because of a confidentiality agreement with the manufacturer. The procedure employed to develop these designs is described in detail in [11] and is based on modified design techniques for induction motors. The stators are based on

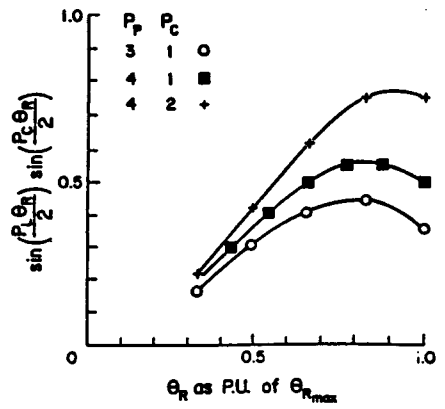

Fig. 5. Rotor cross coupling factor versus rotor loop span angle.

TABLE III
COMPARISON OF BDFM DESIGNS

	3/1 Pole-Pair	4/2 Pole-Pair
Stack Length (mm)	286	286
Stator Frame Size (NEMA)	445	445
Bore Diameter (mm)	361.8	361.8
Stator Slots	72	72
Power Winding		
Voltage (L-L)	460	460
Frequency, Hz	60	60
Coil Pitch	5/6	6/9
Winding Layers	2	2
Turns/Coil	2	3
Coils/Pole/Phase	4	3
Turns/Phase	48	48
Control Winding		
Voltage (L-L)	460 to 40	40 to 460
Frequency	-20 to dc	dc to 30
Coil Pitch	2/3	7/9
Double Layer	2	2
Turns/Coil	4	5
Coils/Pole/Phase	12	6
Turns/Phase	96	72
Rotor		
Diameter (mm)	360.4	360.4
Slots	40	36
Nests	4	6
Loops/Nest	5	3
Slot Width	4.5°	5.0°
Teeth	parallel	parallel
Slot Depth (mm)	15.2	15.2
Nest Ring Width (mm)	15.2	17.8
Nest Ring Height (mm)	20.3	20.3

frames and laminations of conventional induction motors. The stator windings are conventional two layers each (4 layers total) with the control windings located in the bottom of the slots. The rotors utilize custom laminations. The rotor conductors are assumed diecast aluminum with a common endring from an induction motor of the same frame size. The isolated, nested endrings are shown in Fig. 6.

V. PERFORMANCE PREDICTIONS

Using the steady state model developed in [12], motor performance was predicted using a centrifugal pump load torque while trying to maintain unity power factor on the

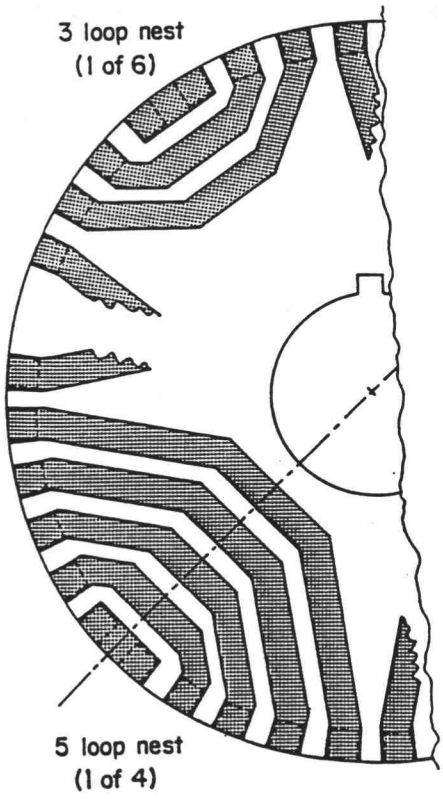

Fig. 6. Rotor nested endrings of the 3/1 and 4/2 BDFMs.

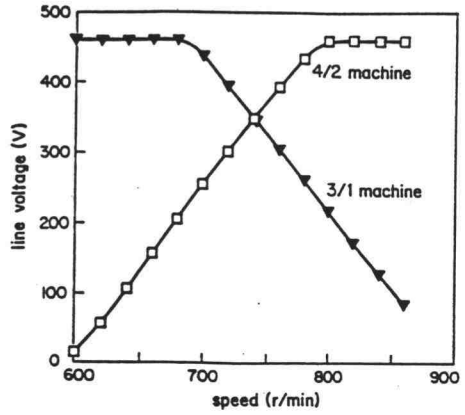

Fig. 7. Control voltage versus speed of the 3/1 and 4/2 BDFMs.

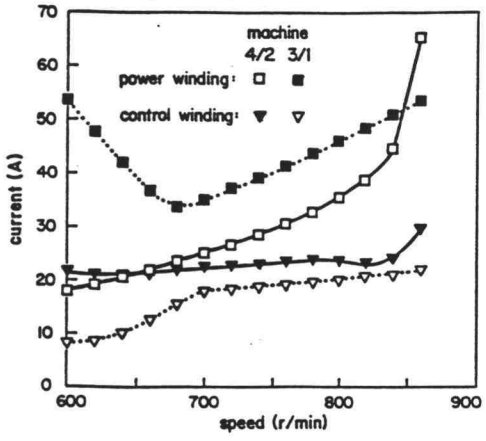

Fig. 8. Control winding phase current predictions of the 3/1 and 4/2 BDFMs.

power winding. The load torque varies from 212 N-m at 600 r/min to 478 N-m at 900 r/min. Efficiencies for the two proposed machines, in excess of 90%, are within five percent of each other throughout the speed range analyzed.

The 4/2 machine uses a positive sequence voltage on the control winding in contrast to the negative sequence voltage used for the 3/1 machine. Because of this, the control voltage maxima occur at opposite ends of the speed range as shown in Fig. 7. The maximum control voltages coincide with maximum control winding frequency in both of the machines owing to the increase in reactance at the higher frequencies.

The control winding phase current predictions, Fig. 8, show that a higher rating converter is needed to drive the 4/2 machine which correlates with the simplistic prediction of converter ratings suggested in (4). However, a smaller rating converter could be used at the cost of reduced power factor at the higher speed range. The power winding current for the 4/2 machine is at a minimum at the low speed due, in part, to the inherently higher torque capabilities of the machine because of its larger number of poles and also because of its better rotor cross coupling factor. However, due to a torque null which occurs at 900 r/min for the 4/2 machine, the stator currents for this machine increase sharply at the high end of the speed range.

The power winding power factors for the machines, Fig. 9, can be maintained at unity with the proper control winding excitation. A drop in power factor occurs if there is insufficient control voltage to excite the machine at the proper level, similar to a conventional synchronous motor. If a unity power factor is not required, perhaps due to existing power factor correction devices, the rating of the converter can be reduced.

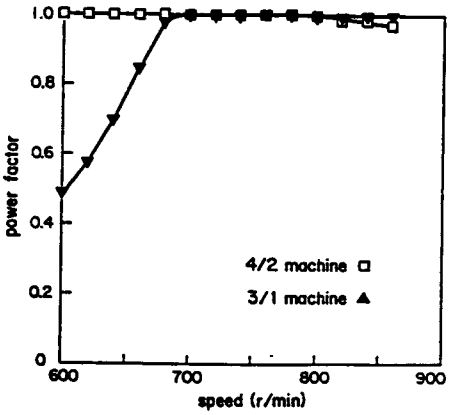

Fig. 9. Power winding power factors of the 3/1 and 4/2 BDFMs.

VI. Conclusions

Potential BDFM designs for a specific speed range can quickly be examined for viability based on the control winding peak frequency from (3); the estimation of converter rating required for unity power factor operation from (4); and the maximum design capability from the rotor cross coupling factor from (6). For a good design, one tries to minimize the peak control frequency required while maximizing the rotor cross coupling factor. The converter rating can be further reduced if unity power factor operation is not required throughout the entire speed range.

Comparison of the BDFM with an adjustable speed induction motor drive shows the superiority of the BDFM in maintaining close to unity power factor using a substantially decreased rating of power converter and similar voltage/frequency control algorithm.

For the pump drive application investigated, several tradeoffs regarding speed capability, converter rating, and power factor need to be made. Both the 4/2 and the 3/1 prove to be good candidates for the application investigated. However, the 4/2 suffers from a null in the torque speed curve at 900 r/min which may preclude its use in this application unless a lower speed of 860 r/min is adequate. In its favor is the ability to maintain near unity power factor throughout its usable speed range in contrast to the lower power factor of the 3/1 machine in the lower speed range.

VII. Acknowledgements

The authors wish to acknowledge funding of the BDFM research project from Electric Power Research Institute, Bonneville Power Administration, and Puget Sound Power and Light.

VIII. References

[1] Y. Liao and C. Sun, "A Low Cost, Robust Sensorless Controlled Scheme for Doubly-Fed Reluctance Motor Drives," *IEEE Industry Applications Society Annual Meeting Conference Record*, pp. 437-444, 1993.

[2] A. Kusko and C.B. Somuah, "Speed Control of a Single-Frame Cascade Induction Motor with Slip Power Pump Back," *IEEE Trans. on Industry Applications*, IA-14(2), pp. 97-105, April/May 1978.

[3] A.K. Wallace, R. Spée, and H.K. Lauw, "The Potential of Brushless Doubly-Fed Machines for Adjustable Speed Drives," *IEEE Industry Application Society Pulp and Paper Industry Annual Conference*, Seattle, June 20-22, 1990.

[4] C. Brune, R. Spée, and A.K. Wallace, "Experimental Evaluation of a Variable Speed, Doubly-Fed Wind Power Generation System," *IEEE Industry Application Society Annual Meeting Conference Record*, pp. 480-487, 1993.

[5] Y. Xu and Y. Tang, "A Novel Wind Power Generating System Using Field Orientation Controlled Doubly-Fed Brushless Reluctance Machine," *IEEE Industry Application Society Annual Meeting Conference Record*, pp. 408-413, 1992.

[6] L.J. Hunt, "A New Type of Induction Motor," *J. of IEE*, 39, pp. 648-667, 1907.

[7] A.R. Broadway and L. Burbridge, "Self-Cascaded Machine: A Low Speed Motor or High-Frequency Brushless Alternator," *IIE Proc.*, 117(7), pp. 1277-1290, 1970.

[8] R. Li, A.K. Wallace, R. Spée, and Yixin Wang, "Two Axis Model Development of Cage Rotor Brushless Doubly-Fed Machines," *IEEE Trans. on Energy Conversion*, 6(3), pp. 453-460, September 1991.

[9] R. Li, A.K. Wallace, and R. Spée, "Dynamic Simulation of Cage Rotor Brushless Doubly-Fed Machines," *IEEE Trans. on Energy Conversion*, 6(3), pp. 445-452, September 1991.

[10] R. Spée, A.K. Wallace, and H.K. Lauw, "Simulation of Brushless Doubly-Fed Drives," *IEEE Industry Application Society Annual Meeting*, San Diego, 1989.

[11] A.K. Wallace, R. Spée, and A. Alajmi, "A Design for the Brushless Doubly-Fed Machine Adjustable Speed Drive," to be presented at *ICEM*, 1994.

[12] A.K. Wallace, R. Spée, M.S. Boger, and R. Li, "General Pole Number Model of the Brushless Doubly-Fed Machine," *IEEE Industry Applications Society Annual Meeting*, Denver, 1994.

[13] B. Gorti, D. Zhou, R. Spée, G.C. Alexander, and A.K. Wallace, "Development of a Brushless Doubly-Fed Machine for a Limited Speed Pump Drive in a Waste Water Treatment Plant," *IEEE Industry Applications Society Annual Meeting*, Denver, 1994.